Title
A Study of Respiratory Turbinal Morphology in Response to Evolutionary Pressure and Development

Author
Pang, Benison

Publication Date
2017

Peer reviewed|Thesis/dissertation

UNIVERSITY OF CALIFORNIA

Los Angeles

A Study of Respiratory Turbinal Morphology in Response to Evolutionary Pressure and Development

A dissertation submitted in satisfaction of the requirements for the

degree Doctor of Philosophy in Biology

by

Benison Pang

2017

ABSTRACT OF THE DISSERTATION

A Study of Respiratory Turbinal Morphology in Response to Evolutionary Pressure and Development

by

Benison Pang

Doctor of Philosophy in Biology

University of California, Los Angeles, 2017

Professor Blaire Van Valkenburgh, Chair

Although the respiratory turbinals are structures which have long been known to function in heat and water recovery during nasal respiration, the role of natural selection and development in influencing the morphology of these specific turbinals have not been well-studied. With the aid of modern techniques such as computed tomography (CT scanning) and fluid flow models as well as histological analysis, we are now able to quantify and describe the function of respiratory turbinals to a greater degree than ever before. In this dissertation, we examine the morphology and functional significance of the respiratory turbinals at the individual, intraspecific, and interspecific levels. In chapter 1, the constraints of external skull morphology on turbinal form are examined using histological analysis and fluid models, with the goal of challenging conventional assumptions of what structures constitute the respiratory turbinals. In chapter 2, we

compared two populations of a single species of deer mice, in order to assess the plasticity of respiratory turbinals in response to local environmental stress; here, high altitude and concurrent temperature and water stress. As respiratory turbinals are known to vary across species but not within species (in mammals), this chapter offers a first look at the plastic nature of respiratory turbinal development. Finally, in chapter 3, we address the question of whether there is a potential convergence upon an optimum respiratory turbinal size across distantly related phylogenetic groups. To answer this question, we quantified and compared relative respiratory turbinal size in ungulates and carnivorans, which have been previously known to have significantly different turbinal morphology. Further, we also assess the impact of diet on respiratory turbinal morphology within ungulates, as there are different degrees of water stress associated with dietary types. In summary, this dissertation demonstrates that at both the intraspecific and interspecific level, respiratory turbinal morphology in mammals is significantly influenced by lineage-independent factors such as environment stress, as well as lineage-dependent factors such as external skull morphology and diet.

The dissertation of Benison Pang is approved.

David K. Jacobs

Marcus L. Roper

Blaire Van Valkenburgh, Committee Chair

University of California, Los Angeles

2017

DEDICATION

I dedicate this work to my family and friends. To the Habitat crew, I would not have made it through undergrad and grad school without you! Special shoutout to **Eric**; you were my mentor in many ways, and someone I look up to greatly to this day. Thanks for being my partner and for including me in your family. Also special thanks to **Stephen**, thank you for taking care of me in El Salvador. **Mr and Mrs Lam**, thank you for adopting me every year for Thanksgiving and making me feel like part of the family. I am proud to be your adopted son, among your many, many children. **James Gov**, we've been friends since the rock-climbing days, and I'm glad that you and I are still killing zombies together. Among all of my friends I rank you most likely to actually read this dissertation, I hope you enjoy it! **Amanda Desowitz**, I thank fortune for sending you my way that overcast day to try hanging out with a bunch of a weirdos. Our cooking adventures are some of my favorite memories from college, and in my mind you're still the finest slackliner I'll ever meet. I'm proud to know you and be your friend.

To my parents, I owe you an immense debt for being willing to send me overseas for college, when I know you would have preferred me to stay close. Your support through the years has been unconditional, and I am grateful for the trust you placed in me to forge my own path. Thank you both for being incredible role models in life, and for being pillars of support and encouragement whenever I needed it. To Naree, thanks for always keeping me grounded, and supporting me even though you have no idea what I actually do (much like I don't really know what you do either).

To **Caitlin**, I cannot put in words how grateful I am to have met you during the course of this dissertation and for all your support, both emotional and academic. Thank you for being in my life for the past several years, and for the years yet to come!

TABLE OF CONTENTS

LIST OF TABLES

LIST OF FIGURES

ACKNOWLEDGEMENTS

I would like to thank **Dr. Blaire Van Valkenburgh** for being an amazing mentor, and being someone who I am honored to have worked with. Over the last few years, I knew I could always count on you to provide a boost when necessary, be it in the form of encouragement or intellectual discussion which invariably provided much-needed insight into the problem at hand. Most importantly, this dissertation would literally not have been possible without you being in my corner from the start, especially when my admittance to graduate school was in doubt, and for that I will be eternally grateful.

To the Van Valkenburghers, past and present: **Deborah Bird**, you are one of the most singularly unique people I have met in my life, and it is richer for having met you. You are one of my favorite people to talk science with, and among the many things I admire about your scientific mindset is your insistence on understanding fundamentals of any topic. So many times when I thought I understood something, you challenged me to explain it and made me realize that I had some ways to go. Your incredible talent for personable communication is something I will likely never match, but I will try my best. **Caitlin Brown**, if I had to pick a single talent I most admire (and it is hard to pick from so many), I would pick your talent for critical thinking; it manifests so often, particularly in your ability to pull disparate threads of knowledge together into a new stream of thought. **Mairin Balisi**, I greatly admire your methodical nature when it comes to science; never have I come away from your talks without thinking that you have done everything in your power to answer a question you were interested in. As someone who tends to want to take shortcuts, you are someone I strive to emulate in that regard. On social issues, you are also one of, if not the most nuanced, intellectual and eloquent people I have ever met. I'll miss our eating adventures greatly, we had some good times on that front! **Abigail Curtis**, you

took a stand on my behalf when I was but an undergrad, and I thank you greatly for that. **Graham Slater**, you were an invaluable resource on my first paper, and you remain my scientific idol in terms of your ability to concisely and clearly explain anything. This was never more evident when you were able to explain complicated statistics in a way that made sense (at the time) to a befuddled undergrad. **Tony Friscia**, your insightful critiques benefitted each and every one of us, which speaks to your wide-ranging knowledge and understanding of a diverse array of topics. Also, thank you for bringing levity and groundedness to many discussions during lab meetings; it was always a pleasure having you there, and lab meetings were notably drier without your presence and booming laughter.

To my doctoral committee: **David Jacobs**, **Michael Alfaro**, and **Marcus Roper**, thank you for your advice and support. To **Dan Blumstein**, my experience with marmot research is what solidified my interest in EEB. Thank you for the amazing opportunity that set me on this path, and is still one of the favorite things I have ever done.

Brent Craven, thank you for hosting me at Pennsylvania State University and the mentorship you provided during that summer. Working with you has led to some of the more interesting findings that I am proud of reporting in this dissertation.

Jocelyn Yamadera, you merit a special mention for being one of the kindest, most incredible people I have met in my PhD journey. My international status caused you no small amount of headache, but you dealt with it all with a smile, and talking to you was always a high point of my day. My only regret with you is that I didn't buy you flowers more often! On the financial front, I owe **Ora Rutherford-Green** and **Ruth Olivas** a massive debt (pun intended). You were so patient with me despite my difficult financial status and absent-mindedness probably making you wanting to tear your hair out. Thank you for your patience!

Chapter 1 has been published in the Journal of Experimental Biology, with special thanks going to Brent Craven, Karen Yee, Fritz Lischka, Nancy Rawson, Mark Haskins, Charles Wysocki, and Blaire Van Valkenburgh. Chapters 2 and 3 of this dissertation are being prepared to submit for publication with myself as first author, and Blaire Van Valkenburgh as principal investigator. Jay Storz at University of Nebraska-Lincoln and Christine Janis at Brown University have provided invaluable assistance and preliminary data. Kiara Mayo and Ian Farnkopf contributed to lab work. This research was funded by the National Institutes of Health and National Science Foundation.

VITA

EDUCATION

Doctor of Philosophy in Biology at the University of California, Los Angeles, September 2012-Present. Expected 2017. Dissertation Title: A Study of Respiratory Turbinal Morphology in Response to Evolutionary Pressure and Development

Bachelor of Science at the University of California, Los Angeles, 2011.

PUBLICATIONS

Pang B, Yee K, Lischka F, Rawson E, Haskins M, Wysocki C, Craven B, Van Valkenburgh B. 2016. The influence of nasal airflow on respiratory and olfactory epithelial distribution in felids. *Journal of Experimental Biology*. **219**, 1866-1874.

Van Valkenburgh B, **Pang B**, Bird D, Curtis A, Yee K, Wysocki C, Craven B. 2014. Respiratory and olfactory turbinals in Feliform and Caniform carnivorans. *The Anatomical Record*. **297**, 2065-2079.

Bird D, Amirkhanian A, **Pang B**, Van Valkenburgh B. 2014. Quantifying the cribriform plate: influences of allometry, function and phylogeny. *The Anatomical Record*. **297,** 2080-2092.

Monclús R, **Pang B**, Blumstein D. 2014. Yellow-bellied marmots do not compensate for a late start: the role of maternal allocation in shaping life-history trajectories. *Evolutionary Ecology*. **28**, 721-733.

Ranslow AN, Richter JP, Neuberger T, **Pang B**, Van Valkenburgh B, Ryan TM, Stecko TD, Craven BA. 2014. Reconstruction and morphometric analysis of the nasal cavity of the white-tailed deer (*Odocoileus virginianus*) and implications regarding respiratory and olfactory airflow. *The Anatomical Record*. **297**, 2138-2147.

Green P, Van Valkenburgh B, **Pang B**, Bird D, Rowe T, Curtis A. 2012. Respiratory and olfactory turbinal size in canid and arctoid carnivorans. *Journal of Anatomy*. **221**, 609-621.

PRESENTATIONS

January 2013 Annual Meeting of the Society for Integrative and Comparative Biology (SICB). Poster Presentation Title: "Comparison of Nasal Turbinal Surface Area in Caniform and Feliform Carnivorans"

January 2012 Annual Meeting of the Society for Integrative and Comparative Biology (SICB). Poster Presentation Title: "Respiratory and Olfactory Turbinate Size in Canid and Arctoid Carnivorans"

APPOINTMENTS

Teaching Assistant, Department of Ecology and Evolutionary Biology, University of California, Los Angeles. 2011-2017.

Research Assistant, Blumstein Laboratory, University of California, Los Angeles. 2009.

CHAPTER 1

The Influence of Nasal Airflow on Respiratory and Olfactory Epithelial Distribution in Felids

Introduction

Mammals vary widely in their reliance on olfaction, ranging from those with very limited or no sense of smell, as is the case in cetaceans (Godfrey et al., 2013), to those with reduced abilities such as semi-aquatic seals or sea lions (Negus, 1958) and visually dominant species (Schreider and Raabe, 1981; Proctor, 1982; Smith et al., 2004; Hornung, 2006; Smith et al., 2007a; Smith and Rossie, 2008), to those with enhanced abilities such as terrestrial caniforms (e.g., canids, ursids) (Pihlström, 2008; Craven et al., 2007; Van Valkenburgh et al., 2011). To understand the evolution of this variation, it is useful to estimate olfactory ability across a wide range of species, both extant and extinct. To do so, investigators have relied on osteological proxies of olfactory ability, such as olfactory bulb size (Healy and Guilford, 1990), ethmoid plate surface area (Bhatnagar and Kallen, 1974; Pihlström et al., 2005; Pihlström, 2008, Bird et al., 2014) or the area of the nasal cavity covered in olfactory epithelium (OE) (Negus, 1958; Wako et al., 1999; Rowe et al., 2005; Van Valkenburgh et al., 2011; Green et al., 2012). The latter is typically estimated from the surface area of the ethmoturbinals and frontoturbinals, a connected set of bony scrolls that are largely housed within the caudal-most aspect of the nasal cavity. This is based on the assumption that the ethmoturbinal and frontoturbinal scrolls are covered in sensory (olfactory) epithelium to the same degree in all species.

However, recent histological studies have shown that while this assumption may hold for species with a long snout, it is not true of short-snouted species, such as small primates, bats, and at least one marsupial (Rowe et al., 2005; Smith et al., 2007a, 2007b, 2012). In these species, the first ethmoturbinal (Maier, 1993; Smith and Rossie, 2006) extends far forward in the

foreshortened nasal cavity, placing it within the respiratory airflow path, where it is covered in respiratory rather than OE. Thus, the surface area of the ethmoturbinals is an overestimate of olfactory surface area (and presumably ability) in these species. Similarly, estimates of the surface area available for heat and moisture transfer during respiration based solely on the maxilloturbinals will be underestimated.

In addition to the aforementioned osteological proxies of olfactory ability, recent studies (Craven et al., 2007, 2010; Lawson et al., 2012) have demonstrated that the anatomical structure of the nasal cavity and the resulting intranasal airflow and odorant deposition patterns may also contribute significantly to olfactory ability. Specifically, Craven et al. (2007, 2010) suggested that two key features of the nasal cavity in keen- scented (macrosmatic) animals (including carnivorans) are the presence of a dorsal meatus, which functions as a bypass for airflow around the maxilloturbinals, and a posteriorly-located olfactory recess that may be partially or entirely separated from the respiratory airflow path by a thin plate of bone called the transverse lamina (Negus, 1958). As a result of this nasal morphology, airflow in the canine nose was shown to split into distinct respiratory and olfactory flow paths, in which olfactory airflow is directed through the dorsal meatus to the posterior olfactory recess, where it then slowly flows anteriorly through the fronto-ethmoturbinal complex, eventually reaching the nasopharynx and exiting the nasal cavity (Craven et al., 2010). Additionally, Craven et al. (2010) postulated that since macrosmatic animals (e.g., carnivorans, ungulates, rodents, marsupials) all appear to possess a common gross nasal architecture consisting of a dorsal meatus and an olfactory recess, similar nasal airflow patterns might be expected in these species. Nasal airflow studies in the rat support this assertion (Kimbell et al., 1997; Zhao et al., 2006; Yang et al., 2007a). In contrast, airflow patterns in the feeble-scented (microsmatic) human nasal cavity, which lacks a dorsal meatus and

an olfactory recess, vary significantly from those in macrosmatic species, largely because the olfactory region in humans is situated within the main respiratory airflow path through the nasal cavity (e.g., see Keyhani et al., 1995; Subramaniam et al., 1998; Zhao et al., 2004; Zhao et al. 2006).

Although felids are considered to be macrosmats relative to primates, including humans, they are similar to non-human primates in having reduced snout lengths. An earlier study that estimated respiratory turbinal size in canids and felids, based on maxilloturbinal bone volume, found that felids have reduced maxilloturbinals relative to canids (Van Valkenburgh et al., 2004). By itself, this finding suggests a reduced ability to condition inspired air as well as retain heat and water relative to canids, but this seems unlikely given that canids and felids share similar environments and have widely overlapping geographic ranges. Instead, it may be that, as in other short-snouted mammals, the anterior ethmoturbinals have been recruited to participate in respiration rather than olfaction. To explore this possibility, we analyzed the distribution of OE vs. nonsensory epithelium in the nasal cavity of the domestic cat, Felis catus, using standard histological techniques and compared this to a similar analysis of the bobcat, Lynx rufus (Yee at al., in press). To better understand the relationship between tissue distribution and cranial anatomy in three dimensions, we matched selected slices from CT scans of a domestic cat skull to our histological sections, and highlighted regions covered by OE and nonsensory epithelia on the CT scans. We also performed a computational fluid dynamics (CFD) simulation of nasal airflow in the bobcat to assess the correlation between airflow patterns and epithelial distribution on the turbinals.

MATERIALS AND METHODS

Animal and tissue collection

For the domestic cat, we sampled two adults, a 10-year old male with normal genotype and phenotype (#4298) and a 6.5 month old male (#6559) heterozygous for a mucopolysaccharidoses VI genotype and normal phenotype. Histological samples were obtained at autopsy from cats housed at the University of Pennsylvania, School of Veterinary Medicine, and euthanized with an overdose (80 mg/kg) of pentobarbital in accordance with protocols approved by its Institutional Animal Care and Use Committee and the guidelines of the American Veterinary Medical Association. Experiments described in this work conformed to the National Institutes of Health guide for the care and use of laboratory animals (NIH Publications 80-23, revised 1978). The anterior portion of each head containing the nose and olfactory bulbs was removed and fixed in 4% paraformaldehyde in phosphate buffered saline for seven days, beginning 15-30 minutes after euthanasia. After seven days of fixation, the heads were decalcified in Sorenson's solution (5% ethylenediaminetetraacetic acid (EDTA) in phosphate buffer, pH = 6.8), and then cryoprotected in 10%, 20%, and 30% sucrose series. The lower jaws and muscles were removed and the noses were frozen in M1 embedding matrix (Shandon Lipshaw, Pittsburgh, PA). A series of coronal sections (16-20 μm) were made at various intervals. Sections were placed onto Superfrost Plus slides (Fisher Scientific, Pittsburgh PA) or Starfrost Adhesive slides (Mercedes Medical, Sarasota FL) and stored at –80°C.

For the bobcat, a single adult specimen was acquired from a trapper in Pennsylvania in accordance with the regulations of the Pennsylvania Game Commission.

The head was removed and the nose was flushed with 4% paraformaldehyde, and was then placed in the same fixative solution for approximately two weeks at 4°C. The specimen was then immersed for another two weeks in a phosphate-buffered saline solution containing

approximately 0.25% Magnevist (Bayer, Germany) for high- resolution magnetic resonance imaging (MRI) scanning. After MRI scanning of the nasal cavity was completed, the specimen was then shipped to Monell for histological analysis. As described in Yee at al. (in press), the head was immersed in a decalcification HCl- ETDA buffer solution (Mercedes Medical) after removing the skin and soft tissues surrounding the nose and skull, and stored at 4°C for six weeks, with changes of solution every three to four days. The nose was then further cleaned by removing the teeth, lower jaw, orbital bones and posterior regions of the skull. The nose was bisected into sagittal halves and the right side was used for histological analysis.

Histological Staining

Domestic cat slides were initially dried in an oven at 56°C overnight. After rehydration with dH2O, slides were stained with Alcian Blue at pH 2.5 for 10 minutes (Fisher Scientific) to label goblet cells and Bowman's glands, rinsed three times with dH2O, followed by nuclear fast red (Vector Laboratories, Burlingame, CA, USA) for 3-4 minutes. After rinsing three times with dH2O, the slides were dried in an oven for one hour and cleared with Histoclear (National Diagnostics, Atlanta GA) and mounted on glass coverslips with Permount (Fisher Scientific). For cat #4298, 65 slides at intervals between 160-200 μm were stained. Of those, 26 stained sections, between 0.5-2.5 mm apart, were selected for quantitative measurement with the most anterior section at approximately 14 mm posterior to the tip of the nose and the last section at a distance of 43.45 mm from the tip of the nose. For cat #6559, 26 stained slides, between 0.3 - 2.6 mm apart, with similar turbinal anatomy to that in the selected sections from cat #4298, were chosen for staining and quantitative analysis.

For the bobcat, 21 slides at intervals from 200-400 μm were stained with Alcian blue and nuclear fast red. To further visualize OE from nonsensory epithelium, adjacent sections were labeled with β-tubulin III antibody, as has been previously done to label olfactory neurons in cats (Lischka et al., 2008). After washing, tissue sections were incubated with a secondary mouse biotinylated antibody (Vector Laboratories), followed by the avidin-biotinylated horseradish peroxidase complex ABC Elite Kit (Vector Laboratories). Sections were then reacted with the chromogen diaminobenzidine (DAB; Sigma Chemicals) and 0.1% H2O2 for visualization.

Quantitative Measurements of Histological Sections

For the domestic cats, selected stained sections were digitally scanned at 1200 dpi resolution on a HP flatbed scanner to generate an 8" x 10" printed hard copy of each section. For the bobcat, stained sections were digitally captured with a RT slider SPOT camera (Diagnostic Instruments, Inc) attached to a Nikon SMZ-U dissecting microscope. The septum, maxilloturbinal, nasoturbinal, and fronto-ethmoturbinals were identified based on location in each section. Nonsensory epithelium (including respiratory, transitional, and stratified epithelia) and OE were identified under 40X and 60X objective magnifications by well-defined histological characteristics of olfactory mucosa as contrasted to the adjacent respiratory mucosa (i.e., epithelial thickness, presence or absence of Alcian blue stained goblet cells and/or Bowman's glands in the underlining lamina propria). For the cats, OE was identified via well-defined histological characteristics (as described). For the bobcat, OE was identified by β-tubulin labeling.

Digital scans of the domestic cats and bobcat were quantitatively measured using the ImageProPlus 6.0 software (MediaCybernetics). The following measures were taken on each

section for both sides of the cat noses and the right side of the bobcat nose: 1) the total length (cross-sectional perimeter) of the septum, maxilloturbinals, nasoturbinals, and fronto-ethmoturbinals, respectively and 2) the total length (cross-sectional perimeter) of OE lining each of these structures. Our measurement of the fronto-ethmoturbinal complex includes all larger and smaller turbinals of the ethmoid bone (i.e., combined surface area of the ethmoturbinals, interturbinals, and frontoturbinals as defined by Maier, 1993; Smith et al., 2007b; Maier and Ruf, 2014). The perimeter of nonsensory epithelium for each section was determined by subtracting OE perimeter from total septal and turbinal perimeters. The surface area of a given section was calculated by multiplying the perimeter of OE for a section by the distance to the next section. The OE surface areas were summed across all sections to give a cumulative measure of OE surface area on the nasoturbinals, septum, and fronto-ethmoturbinals. With these measurements, we also calculated the proportion of the surface area of the turbinals and septum that are covered with OE, as well as the relative OE/nonsensory epithelium ratio in the nasal fossa. As the bobcat measurements were taken from the right half of the nose, cumulative measurements from the domestic cats were divided by two to allow for a consistent comparison.

Because the anterior tips of turbinals may have been excluded if they occurred in the interslice intervals (0.2 – 0.4mm), we estimated the maximum possible error. This was done by adding the perimeter of OE measured on its first occurrence to the overall sum of OE on the septum, nasoturbinals, fronto-ethmoturbinals and cumulative total OE respectively, and found the percentage difference that arose from this addition. The maximum OE perimeter measurement error due to possibly excluding the anterior tips of turbinals and septum because

they ended in an interslice interval was, on average, 4.8% for the septum, 12.7% for the nasoturbinals, 0.04% for the ethmoturbinals, and 2.1% for the cumulative total OE surface area.

CT scans

To view the anatomy in three dimensions, high-resolution CT (HRCT) scans of the skull of a domestic cat (Felis catus) were acquired at The Pennsylvania State University (PSU). The data set comprises 387 scans of the nasal cavity, with a slice thickness of 0.238 mm, and is available by request from the Digimorph library (http://www.digimorph.org/). The scans were first imported into the software program Mimics 14.0 (Materialise Inc.) to view the three-dimensional data set from coronal, sagittal, and transverse perspectives, as well as to enhance visualization of the turbinals by increasing the contrast between the bony turbinals and the air. Coronal CT scans were selected where the morphology of the turbinals most closely resembled histological sections at various locations in the nasal fossa (Figs 1-3). This allowed for a comparison of the relative distributions of epithelium at specific locations in the nasal fossa. To compare the degree of overlap of the fronto-ethmoturbinals and maxilloturbinals between a long-snouted canid and a short-snouted felid, CT scans of the skull of a Mexican gray wolf (Canis lupus baileyi) (USNM 98307, Smithsonian Institution, Washington, D.C.) were also obtained from the University of Texas and processed the same way as the scans of the domestic cat. A similar procedure was performed for two additional felids, the cheetah (Acinonyx jubatus, FMNH 29635, Field Museum of Natural History, Chicago) and the African lion (Panthera leo, MMNH 17537, University of Minnesota Museum of Natural History, Minneapolis). Subsequently, we inspected sagittal scans of the nasal fossa of each animal to estimate the degree of overlap in each case.

Computational fluid dynamics

To examine nasal airflow patterns in a short-snouted felid, we acquired high- resolution (80 μ m isotropic) MRI scans (Fig. 4A, B) of the head of the bobcat at PSU and reconstructed a three-dimensional anatomical model of the left nasal airway (Fig. 4C) from the MRI data using the methodology of Craven and colleagues (Craven et al., 2007; Ranslow et al., 2014; Coppola et al., 2014). A high-fidelity, hexahedral-dominant computational mesh (Fig. 4D) was then generated from the reconstructed nasal airway surface model using snappyHexMesh, the unstructured mesh generation utility in the open-source computational continuum mechanics library OpenFOAM (www.openfoam.com). The mesh contained roughly 121 million computational cells, including five wall-normal layers along the airway walls to resolve near-wall velocity gradients and a spherical refinement region around the nostril to resolve the flow as it accelerates toward and enters the naris on inspiration.

A steady-state computational fluid dynamics (CFD) simulation of laminar airflow during inspiration was performed using OpenFOAM. As in Craven et al. (2009), the computational domain included the anatomical model of the left nasal airway positioned in the center of a large rectangular box with atmospheric pressure boundary conditions assigned to the sides of the box. A pressure outlet boundary condition was specified at the nasopharynx to induce a physiologically realistic respiratory airflow rate of 3.7 l/min, which was determined from the mass of the specimen (12 kg) and the allometric equation for respiratory minute volume developed by Bide et al. (2000). No-slip boundary conditions were assigned on the external nose and airway walls, which were assumed to be rigid. Additionally, as justified by Craven et al. (2009), the presence of the thin mucus layer that lines the nasal epithelium was neglected.

The SIMPLE (Semi-Implicit Method for Pressure-Linked Equations) algorithm was used to numerically solve the incompressible continuity and Navier-Stokes equations using second-order accurate spatial discretization schemes. The simulation was performed on 480 processors of a parallel computer cluster at PSU. Iterative convergence of the SIMPLE algorithm was obtained by forcing the normalized solution residuals to be less than 10-4. Additionally, the volumetric flow rate, viscous and pressure forces, and other solution quantities were monitored to ensure solution convergence. Visualization and post-processing of the CFD results were performed using the open-source visualization software ParaView (www.paraview.org).

RESULTS

In cat #6559, OE was distributed unequally over the septum, nasoturbinals, and fronto-ethmoturbinals. Approximately 24.5% of the total OE could be found on the septum, with 5.3% lining the nasoturbinals, and 70.2% lining the fronto-ethmoturbinals (Table 1.1). This was similar to the distribution in cat #4298, in which 22.1% of total OE was found on the septum, 8% on the nasoturbinals, and 69.9% on the fronto- ethmoturbinals, as well as the bobcat in which 15.8% of total OE was found on the septum, 6.7% on the nasoturbinal, and 77.5% on the fronto-ethmoturbinals. On average, cat #6559 had a cumulative total OE surface area of 839.7 mm2, while cat #4298 had a total of 940 mm2. The bobcat had a cumulative total OE surface area of 2333.9 mm2. Overall, the ratio of OE surface area to nonsensory epithelium surface area was 0.14 in cat #6559, 0.12 in cat #4298 and 0.16 in the bobcat.

In both domestic cats, the general pattern of OE distribution in the nasal fossa was similar, and so here we report the results obtained from cat #6559. In the rostral region, the fronto-ethmoturbinals extended anteriorly in the snout, lying above much of the maxilloturbinal

complex (Fig. 1A). However, the most anterior appearance of OE was not on the fronto-ethmoturbinals. Instead, it first appeared on the roof of the nasal cavity and the dorsal arch of the nasoturbinals, at a distance of about 38% of the total length of the nasal fossa (Fig. 2A). At this location, the maxilloturbinals were barely present. Here, the fronto-ethmoturbinals occupied much of the available space, and were totally covered with nonsensory epithelium.

OE remained concentrated on the septum and the medial aspect of the nasoturbinals for the anterior 60% of the total length of the nasal fossa, at which point it began to gradually expand laterally (Fig. 2B). OE was present posterior to the internal nares within the anterior regions of the olfactory recess, where it was predominantly distributed on the septum, nasoturbinal, and the medial portion of the fronto- ethmoturbinals (Fig. 2C).

Within the caudal regions of the olfactory recess, the proportional coverage of OE increased posteriorly until, at a position of approximately 90% of the total length of the nasal fossa, 48.6% of the available turbinal and septum surface area was covered by OE (Fig. 2D). At location E, at a position of approximately 98% of the total length of the nasal fossa, OE covered 44.5% of the available surface area, with an approximate even split dorsal and ventral to the cribriform plate (Fig. 2E).

In the bobcat, the broad patterns of epithelial distribution (OE and nonsensory) are fairly similar to that of the domestic cat; Figure 3 shows histological outlines and MRI scans of the bobcat nasal cavity at corresponding locations to that of the domestic cat in Figure 2. In the anterior nasal cavity of the bobcat (Fig. 3A), the fronto- ethmoturbinals are present and are covered with nonsensory epithelium much like in the domestic cat. OE is also first seen in the bobcat covering the nasoturbinal and the roof of the nasal cavity. Subsequently, OE is found on the septum and nasoturbinal (Fig. 3B), and only in the olfactory recess (Fig. 3C-E) does OE

occupy a sizeable portion of the available turbinal surface area, which is again comparable to that observed in the domestic cat.

Morphologically, the fronto-ethmoturbinals of the domestic cat extended far forward in the snout and lay above much of the maxilloturbinal complex (Fig. 1A). Compared to the scanned gray wolf, there was much greater overlap of the maxilloturbinal and the fronto-ethmoturbinals in the cat (Fig. 5). Indeed, in sagittal sections it appears that the anterior fronto-ethmoturbinals are aligned with the path of respiratory airflow from the external nares to the nasopharynx, as is the maxilloturbinal. The anterior fronto-ethmoturbinals slope downward posteriorly, appearing to be angled towards the internal nares (Fig. 5). This differs from the alignment of more posterior ethmoturbinals, which are roughly horizontal, particularly in the olfactory recess. A comparison between the relatively long-snouted lion and short-snouted cheetah (Fig. 6) showed a similar result: there was substantially greater overlap of the fronto-ethmoturbinals and maxilloturbinals in the cheetah than in the lion and the anterior fronto-ethmoturbinals also seem to be aligned with the respiratory airflow path.

The CFD simulation of nasal airflow in the bobcat showed that during inspiration, olfactory and respiratory flow paths in the nose are separated; the olfactory flow path passes through the dorsal meatus, directly into the olfactory recess, and subsequently leaves the nasal cavity through the internal nares (Fig. 7). Respiratory airflow, however, does not enter the olfactory recess, but instead flows directly to the internal nares after passing over both the maxilloturbinals and the anterior fronto-ethmoturbinals. Of the two, the anterior fronto-ethmoturbinals comprise a much larger portion of the total respiratory surface area compared to the maxilloturbinals.

DISCUSSION

In general, cats are regarded as macrosmatic animals, though they are thought to have a weaker sense of smell than dogs, based on their behavior and a comparison of the number of functional olfactory receptor genes in both species (Hayden et al., 2010). Cats are carnivorans and as such, possess a macrosmatic nasal airway architecture consisting of a dorsal meatus and an olfactory recess (Figs 1, 2). In this study, we found that this nasal architecture results in a general similarity in the nasal airflow patterns between the bobcat and dog, in that olfactory and respiratory airstreams are separated (see Fig. 7 and Craven et al., 2010, Figure 7). However, unlike the dog, anterior extensions of the fronto- ethmoturbinals spatially overlap the maxilloturbinals in both felids (cat and bobcat) and are covered with respiratory epithelium (Fig. 2A,B; Fig. 3A). In this region, OE is primarily confined to the dorsal meatus, which contains the olfactory airflow stream, while respiratory airflow passes over the (limited) maxilloturbinals and the anterior fronto-ethmoturbinals where OE is absent. Thus, the histological distribution of epithelia in the bobcat nose appears to be highly correlated with the nasal airflow patterns. That is, the respiratory airflow stream passes mainly over nonsensory epithelium, whereas OE is primarily exposed to only the olfactory airflow stream (see Figs. 3 and 7).

Gross nasal morphology and turbinal anatomy in the domestic cat are very similar to that in the bobcat (Figs. 2, 3), which strongly suggests that similar nasal airflow patterns occur in the domestic cat. Given the similar epithelial distribution in the domestic cat and bobcat, the correlation between nasal histology and airflow patterns found in the bobcat also likely applies to domestic cats. Accordingly, these data strongly suggest that the anterior fronto-ethmoturbinals have been co-opted for respiratory function in these two species, and likely other similarly short-snouted felids.

The degree of spatial overlap of the fronto-ethmoturbinals and maxilloturbinals in all three short-snouted felids (domestic cat, bobcat, and cheetah) was similar and much less than that observed in both the longer-snouted lion and the long-snouted gray wolf. This suggests that the degree of spatial overlap of the fronto-ethmoturbinals and maxilloturbinals is more closely correlated with relative snout length than with phylogenetic groupings such as feliforms versus caniforms.

Given the similarity of the gross nasal architecture and the overall nasal airflow patterns between the dog and bobcat, we might also expect qualitatively similar odorant deposition patterns in the olfactory region. Lawson et al. (2012) observed that the highest odorant deposition fluxes are located anteriorly in the sensory region of the canine nose, along the dorsal meatus and nasal septum, which is consistent with our observation of OE being concentrated in this location in the domestic cat (Fig. 2) and bobcat (Fig. 3). In the canine, highly-soluble odorants are deposited anteriorly in the sensory region, particularly along the dorsal meatus, and less-soluble odorants are deposited more uniformly (Lawson et al., 2012). OE in the cats is concentrated on the medial aspect of the olfactory recess, with less OE being distributed peripherally; hence, there is less surface area for detecting moderately-soluble and insoluble odorants. Accordingly, compared with other animals that possess more peripheral OE, cats may have a reduced sense of smell for less soluble odorants.

Compared with other species, it is interesting to note that Smith et al. (2007a, b) also observed respiratory mucosa on fronto-ethmoturbinal I in the mouse lemur (Microcebus murinus) and noted that it is positioned more anteriorly and is, therefore, exposed to respiratory airflow (Smith et al., 2007b). Thus, it appears that fronto- ethmoturbinals in the mouse lemur also may have been co-opted for respiratory air- conditioning. This suggests that fronto-

ethmoturbinals that function in respiration may have arisen convergently in primates and carnivorans as a result of having a shorter snout, either through selection for enhanced jaw muscle leverage in feliforms (Biknevicius and Van Valkenburgh, 1996) or other selection factors that led to reduced primate snouts (Smith et al., 2007b).

In our studies of feliform and caniform carnivorans, there appears to be a clear relationship between turbinal architecture, nasal airflow, and epithelial distribution. Recent research has shown that airflow may influence turbinal size and shape during development (Coppola et al., 2014), which is consistent with the results of this study. Inferring epithelial surface area from CT data alone is difficult, but can be improved by taking into account nasal airflow patterns and the variability of OE distribution in different species. In this study, we have shown that visual inspection of CT data can offer an initial insight into the expected nasal airflow patterns and epithelial distribution. Future work will focus on documenting OE distribution in more short-snouted taxa and testing our hypotheses concerning nasal airflow and odorant deposition patterns using CFD (e.g., as in Zhao et al., 2006; Yang et al., 2007a, b; Craven et al., 2009, 2010; Lawson et al., 2012).

TABLES AND FIGURES

Table 1.1. Calculated OE measurements for all turbinals and septum.

	#6559	#4298	Bobcat
A) Total Surface Area of OE in mm^2 (% of total OE)			
Total OE	839.7 (100%)	940 (100%)	2333.9 (100%)
Total Septum OE	205.7 (24.5%)	207.7 (22.1%)	369.8 (15.8%)
Total Nasoturbinal OE	44.28 (5.3%)	75.4 (8%)	155.3 (6.7%)
Total Fronto- ethmoturbinal OE	589.7 (70.2%)	656.9 (69.9%)	1808.8 (75.5%)
B) Ratio of OE to nonsensory epithelium Total OE/RE	0.14	0.12	0.16

Figure 1.1. Sagittal view of the skull of a domestic cat, with locations A-E indicated to show the location of the scans in Figure 2 within the nasal fossa. Locations defined as the percent of the total length of the nasal fossa from anterior to posterior: A, 38%; B, 60%; C, 80%, D, 93%, and E, 98%.

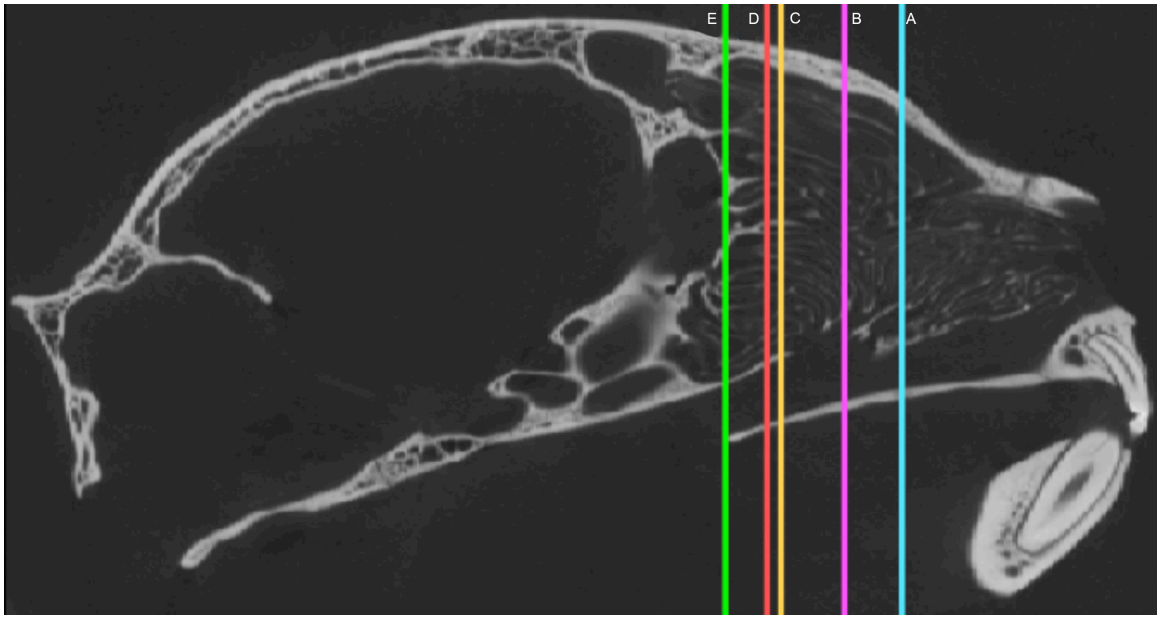

Figure 1.2. Coronal view of histological sections (left) of the turbinals of cat #6559 with OE (purple) and nonsensory epithelium (green), and coronal CT scans (right) corresponding to approximately similar locations in the skull. CT scan A has maxilloturbinals colored in yellow, showing minimal maxilloturbinal presence at this point. Location of scans A-E within the skull as in Figure 1.1.

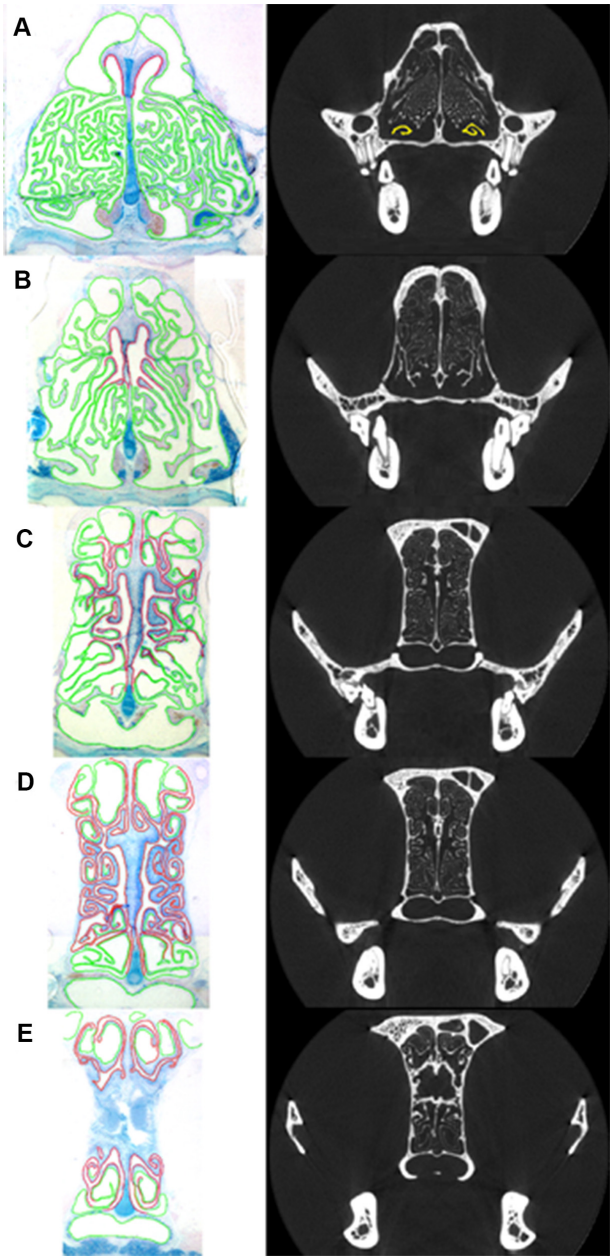

Figure 1.3. Coronal view of histological sections (left) of the turbinals of the bobcat with OE (red) and nonsensory epithelium (green), and coronal MRI scans (right) corresponding to similar locations in the skull. Sections and scans A-E were chosen to approximate those in Figure 2. In section A, MT refers to the maxilloturbinal, FT refers to the fronto-ethmoturbinals, and NT refers to the nasoturbinal. In MRI scan A, the maxilloturbinals have been outlined in yellow.

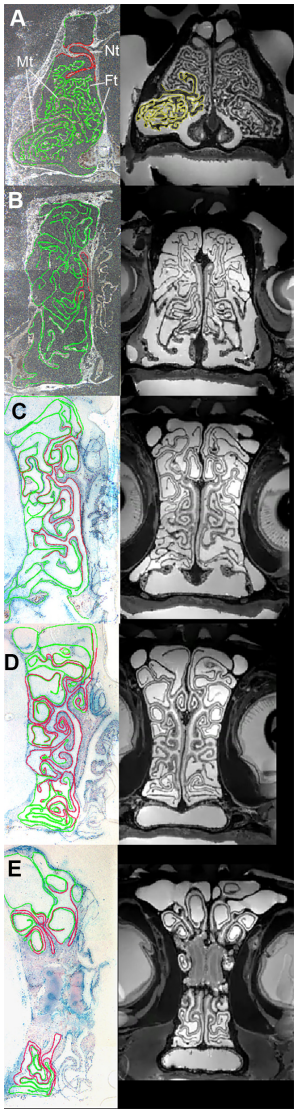

Figure 1.4. Anatomical reconstruction and CFD model of the nasal airway of the bobcat. High-resolution (80 μm isotropic) MRI scans (A, B) of the head of a bobcat cadaver were acquired and

used to reconstruct a three-dimensional anatomical model of the left nasal airway (C). A computational mesh (D) was then generated from the anatomical model and used in a CFD simulation of respiratory airflow in the nose. In the MRI scans (A, B), the airway lumen is light gray, and tissue and bone are dark. In D, the airway is gray.

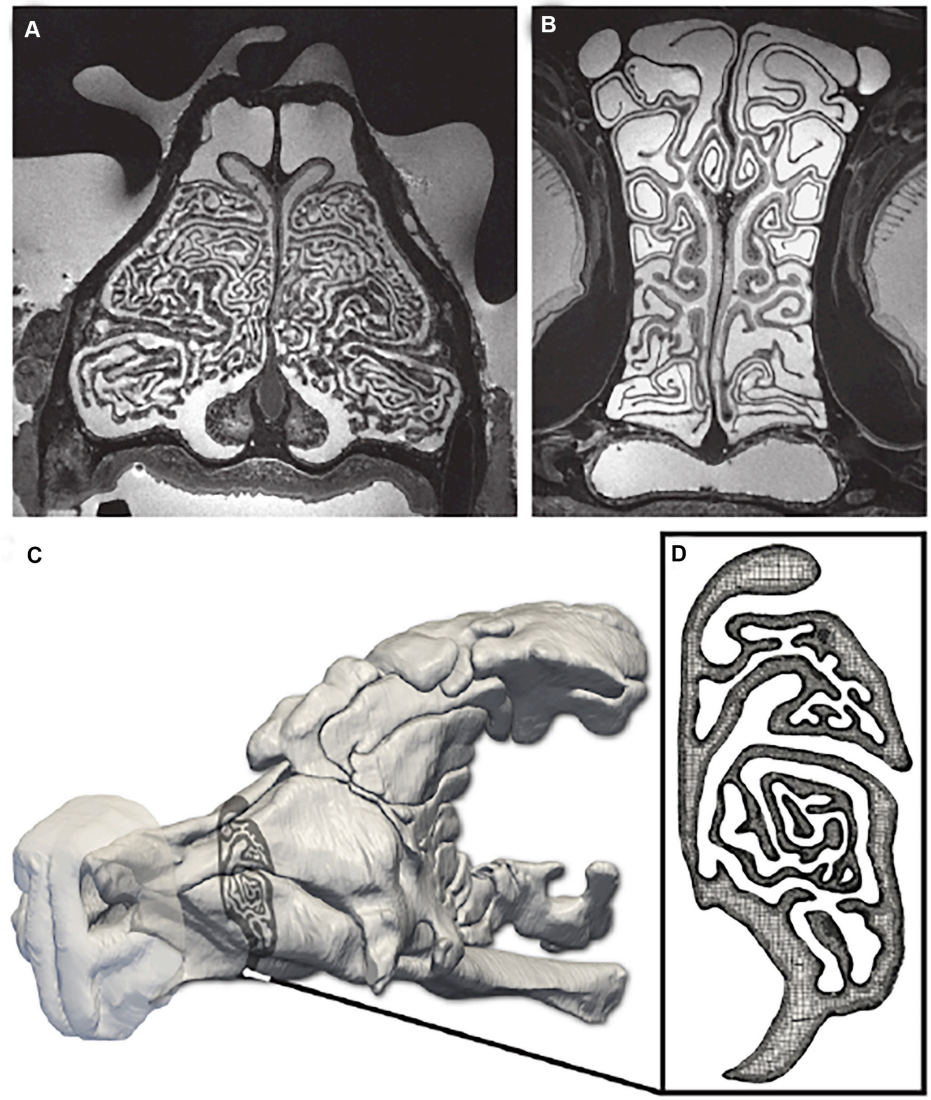

Figure 1.5. Sagittal scans of the turbinals of a domestic cat (Felis catus) and a Mexican gray wolf (Canis lupus baileyi). Ethmoturbinals in red, maxilloturbinals in blue.

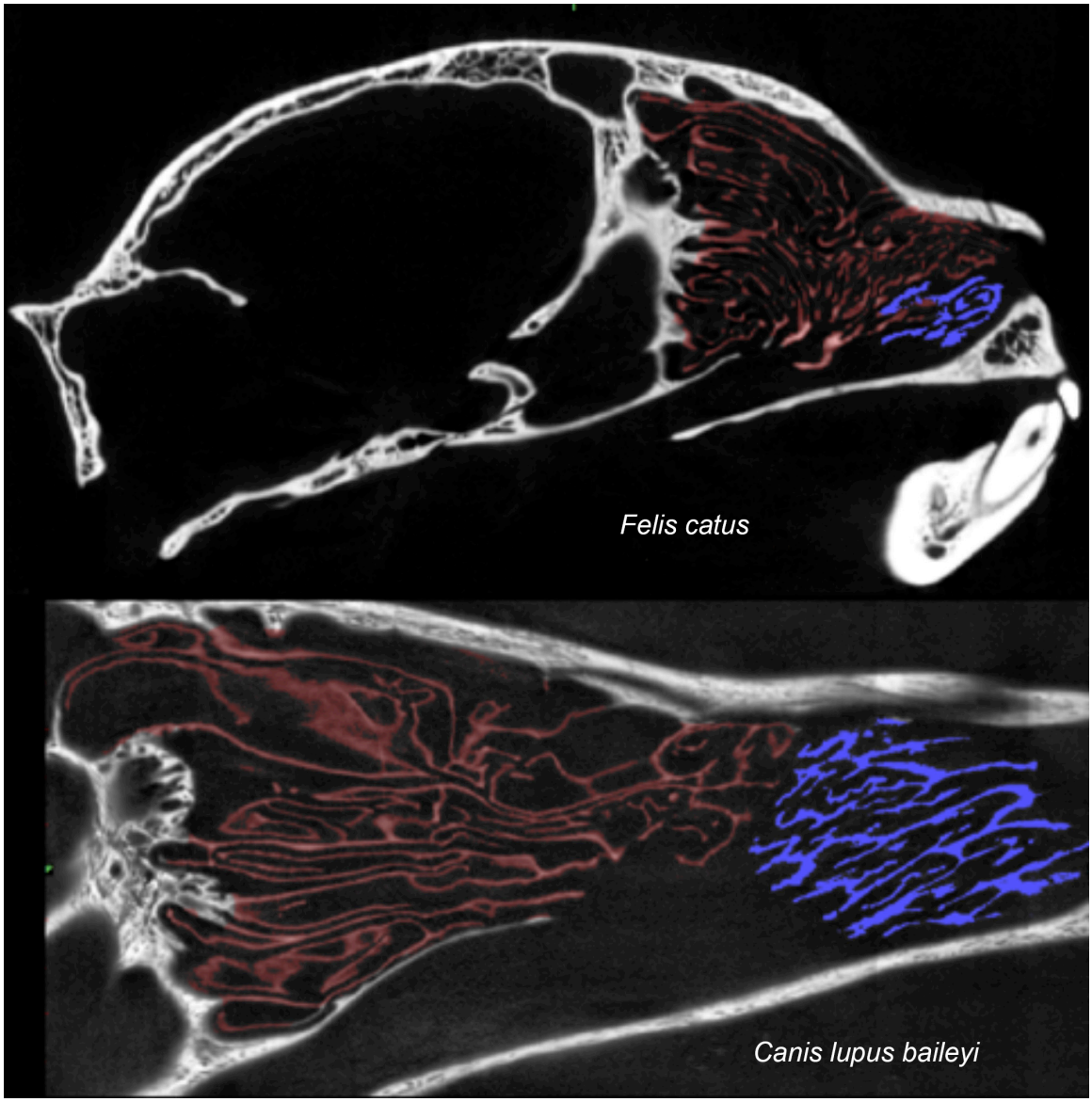

Figure 1.6. Sagittal scans of the turbinals of a cheetah (Acinonyx jubatus) and a lion (Panthera leo). Ethmoturbinals in red, maxilloturbinals in blue.

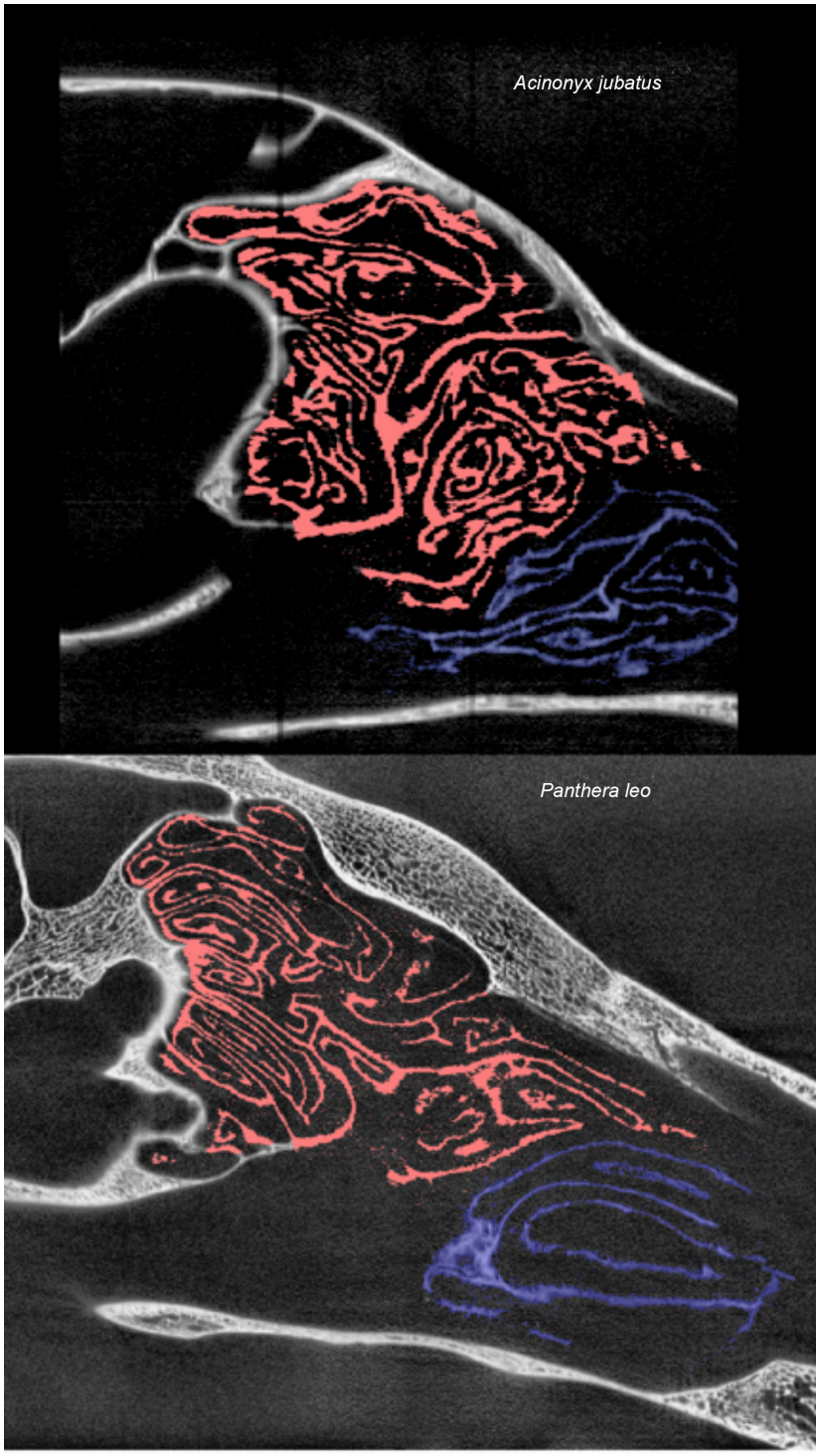

Figure 1.7. Nasal airflow patterns in the bobcat obtained from a CFD simulation of airflow in the nose. The fronto-ethmoturbinals (red) and maxilloturbinals (blue) were segmented from the

MRI data and are visualized with flow streamlines extracted from the CFD solution. As Craven et al. (2010) found in the domestic dog, separate respiratory and olfactory airflow paths exist in the nasal cavity of the bobcat. Olfactory airflow (illustrated by red streamlines) reaches the olfactory recess via the dorsal meatus, bypassing the convoluted maxilloturbinals. Respiratory airflow (illustrated by blue streamlines) is directed away from the olfactory recess and toward the internal nares by the maxilloturbinals and the anterior extensions of the fronto-ethmoturbinals.

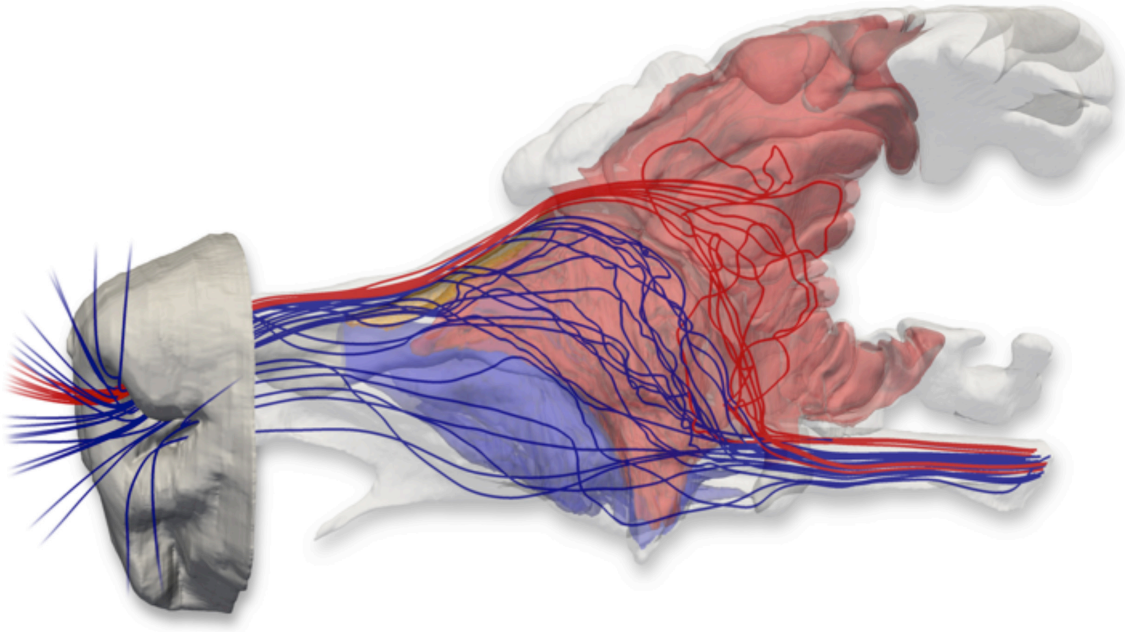

REFERENCES

Bhatnagar KP, Kallen FC (1974) Cribriform plate of ethmoid, olfactory bulb and olfactory acuity in forty species of bats. *Journal of Morphology*, **142**, 71–89

Bide RW, Armour SJ, Yee E (2000) Allometric respiration/body mass data for animals to be used for estimates of inhalation toxicity to young adult humans. *Journal of Applied Toxicology,* **20**, 273–290.

Biknevicius AR, Van Valkenburgh B (1996) Design for killing: craniodental adaptations of predators. In *Carnivore behavior, ecology, and evolution*, Vol. 2 (ed. J. L. Gittleman), pp. 393–428. Ithaca, NY: Cornell University Press.

Coppola DM, Craven BA, Seeger J, Weiler E (2014) The effects of naris occlusion on mouse nasal turbinate development. *The Journal of Experimental Biology* **217**, 2044–2052.

Craven BA, Neuberger T, Paterson EG, Webb AG, Josephson EM, Morrison EE, Settles GS (2007) Reconstruction and morphometric analysis of the nasal airway of the dog (*Canis familiaris*) and implications regarding olfactory airflow. *The Anatomical Record*, **290**, 1325–1340.

Craven BA, Paterson EG, Settles GS, Lawson, MJ (2009) Development and verification of a high-fidelity computational fluid dynamics model of canine nasal airflow. *Journal of Biomechanical Engineering*, **131**, 091002.

Craven BA, Paterson EG, Settles GS (2010) The fluid dynamics of canine olfaction: unique nasal airflow patterns as an explanation of macrosmia. *Journal of the Royal Society Interface*, **7**, 933–943.

Godfrey SJ, Geisler J, Fitzgerald EMG (2013) On the Olfactory Anatomy in an Archaic Whale (Protocetidae, Cetacea) and the Minke Whale Balaenoptera acutorostrata (Balaenopteridae, Cetacea). *The Anatomical Record*, **296**, 257–272.

Hayden S, Bekaert M, Crider TA, Mariani S, Murphy WJ, Teeling EC (2010) Ecological adaptation determines functional mammalian olfactory subgenomes. *Genome Research*, **20**, 1–9.

Healy S, Guilford T (1990) Olfactory-Bulb Size and Nocturnality in Birds. *Evolution*, **44**, 339–346.

Hornung DE (2006) Nasal anatomy and the sense of smell. *Advances in Otorhinolaryngology*, **63**, 1–22.

Keyhani K, Scherer PW, Mozell MM (1995) Numerical simulation of airflow in the human nasal cavity. *Journal of Biomechanical Engineering*, **117**, 429–441.

Kimbell JS, Godo MN, Gross EA, Joyner DR, Richardson RB, Morgan KT (1997) Computer simulation of inspiratory airflow in all regions of the F344 rat nasal passages. *Toxicology and Applied Pharmacology*, **145**, 388–398.

Lawson MJ, Craven BA, Paterson EG, Settles GA (2012) A computational study of odorant transport and deposition in the canine nasal cavity: implications for olfaction. *Chemical Senses*, **37**, 553–566.

Lischka FW, Gomez G, Yee KK, Dankulich-Nagrundy L, Lo L, Haskins ME, Rawson NE (2008) Altered olfactory epithelial structure and function in feline models of mucopolysaccharidoses I and VI. *Journal of Comparative Neurology*, **511**, 360–372.

Maier W (1993) Zur evolutiven und funktionellen Morphologie des Gesichtsschädels der Primaten. *Zeitschrift für Morphologie und Anthropologie*, **79**, 279–299.

Maier W, Ruf I (2014). Morphology of the nasal capsule of primates – with special reference to Daubentonia and Homo. *The Anatomical Record*, **297**, 2018-2030.

Negus V (1958). *The Comparative Anatomy and Physiology of the Nose and Paranasal Sinuses*. Edinburgh: E. & S. Livingstone.

Pihlström H, Fortelius M, Hemilä S, Forsman R, Reuter T (2005) Scaling of mammalian ethmoid bones can predict olfactory organ size and performance. *Proceedings of the Royal Society B*, **272**, 957–962.

Pihlström H (2008) Comparative Anatomy and Physiology of Chemical Senses in Aquatic Mammals. In *Sensory Evolution on the Threshold (ed. J. G. M. Thewissen and S. Nummela)*, pp. 95–109. Berkeley: University of California Press.

Proctor DF (1982) The Upper Airway. In *The Nose: Upper Airway Physiology and the Atmospheric Environment* (ed. D. F. Proctor. and I. H. P. Andersen), pp. 23–43. New York, NY: Elsevier Biomedical Press.

Ranslow AN, Richter JP, Neuberger T, Van Valkenburgh B, Rumple CR, Quigley AP, Pang B, Krane MH, Craven BA (2014) Reconstruction and morphometric analysis of the nasal airway of the white-tailed deer (*Odocoileus virginianus*) and implications regarding respiratory and olfactory airflow. *The Anatomical Record*, **297**, 2138–2147.

Rowe TB, Eiting TP, Macrini TE, Ketcham RA (2005) Organization of the olfactory and respiratory skeleton in the nose of the gray short-tailed opossum *Monodelphis domestica*. *Journal of Mammalian Evolution*, **12**, 303–336.

Schreider JP, Raabe OG (1981). Anatomy of the nasal-pharyngeal airway of experimental animals. *The Anatomical Record*, **200**, 195–205.

Smith, TD, Rossie JB (2006). Primate olfaction: anatomy and evolution. In *Olfaction and the brain: Window to the mind.* (ed. W. Brewer, D. Castle, and C. Pantelis), pp. 135–166. Cambridge: Cambridge University Press.

Smith, TD, Rossie JB (2008). Nasal fossa of mouse and dwarf lemurs (primates, cheirogaleidae). *The Anatomical Record*, **291**, 895–915.

Smith, TD, Bhatnagar KP, Tuladhar P, Burrows AM (2004) Distribution of olfactory epithelium in the primate nasal cavity: are microsmia and macrosmia valid morphological concepts? *The Anatomical Record Part A, Discoveries in Molecular, Cellular and Evolutionary Biology*, **281**, 1173–1181.

Smith, TD, Bhatnagar KP, Rossie JB, Docherty BA, Burrows AM, Cooper GM, Mooney, MP, Siegel MI (2007a) Scaling of the first ethmoturbinal in nocturnal strepsirrhines: olfactory and respiratory surfaces. *The Anatomical Record*, **290**, 215–237.

Smith, TD, Rossie JB, Bhatnagar KP, (2007b). Evolution of the nose and nasal skeleton in primates. *Evolutionary Anthropology*, **16**, 132–146.

Smith, TD, Eiting TP, Bhatnagar KP (2012). A quantitative study of olfactory, non-olfactory, and vomeronasal epithelia in the nasal fossa of the bat Megaderma lyra. *Journal of Mammalian Evolution*, **19**, 27–41.

Subramaniam RP, Richardson RB, Morgan KT, and Kimbell JS (1998) Computational fluid dynamics simulations of inspiratory airflow in the human nose and nasopharynx. *Inhalation Toxicology*, **10**, 91–120.

Van Valkenburgh B, Theodor J, Friscia A, Pollack A, Rowe T (2004) Respiratory turbinates of canids and felids: a quantitative comparison. *Journal of Zoology*, **264**, 281–293.

Van Valkenburgh B, Curtis A, Samuels JX, Bird D, Fulkerson B, Meachen- Samuels J, Slater GJ (2011) Aquatic adaptations in the nose of carnivorans: evidence from the turbinates. *Journal of Anatomy*, **218**, 298–310.

Wako K, Hiratsuka H, Katsuta O, Tsuchitani M (1999) Anatomical structure and surface epithelial distribution in the nasal cavity of the common cotton-eared marmoset (*Callithrix jacchus*). *Experimental Animals*, **48**, 31–36.

Yang GC, Scherer PW, Mozell MM (2007a) Modeling inspiratory and expiratory steady-state velocity fields in the Sprague-Dawley rat nasal cavity. *Chemical Senses*, **32**, 215–223.

Yang GC, Scherer PW, Zhao K, Mozell MM (2007b) Numerical modeling of odorant uptake in the rat nasal cavity. *Chemical Senses*, **32**, 273–284.

Yee, KK, Craven BA, Wysocki CJ, Van Valkenburgh B (2016) Comparative morphology and histology of the nasal fossa in four mammals: gray squirrel, bobcat, coyote and white-tailed deer. *The Anatomical Record*, **299**, 840-852.

Zhao K, Scherer PW, Hajiloo SA, Dalton P (2004) Effect of anatomy on human nasal air flow and odorant transport patterns: Implications for olfaction. *Chemical Senses*, **29**, 365–379.

Zhao K, Dalton P, Yang GC, Scherer PW (2006). Numerical modeling of turbulent and laminar airflow and odorant transport during sniffing in the human and rat nose. *Chemical Senses*, **31**, 107–118.

CHAPTER 2

The Development of the Respiratory Turbinals in Deer Mice (*Peromyscus Maniculatus*) in Response to Stressful Conditions at High Altitude

Introduction

High altitude conditions have long been a point of interest for those interested in the effects of stressful environments on physiology. At high altitudes, hypoxic (low-oxygen) and low-temperature conditions are common, contributing to a highly stressful environment. In humans, studies have found evidence for long-term adaption to high elevation conditions in the indigenous populations of the Andes (Beall, 2006) Tibet (Simonson et al., 2010) and Ethiopia (Beall et al., 2002). Similarly, animals native to high altitude also show adaptations to the stressful conditions. The most commonly observed adaptation to high elevations and concurrent hypoxia is increased hemoglobin-oxygen affinity, as seen in Andean hummingbirds (Projecto-Garcia et al., 2013), Andean waterfowl (Natarajan et al., 2015) and camelids (Reynafarje et al., 1975; Storz, 2007). However, a significantly higher Hb-O_2 affinity is not present in all high altitude species relative to their lowland relatives. Exceptions include snow leopards (Janecka, 2015) squirrels (Revsbech et al., 2013), and pikas (Tufts et al., 2015).

Rodents have been the subject of a significant proportion of the research on high altitude adaptations in mammals, with deer mice (*Peromyscus maniculatus*) a species of particular interest. *P. maniculatus* has one of the largest altitudinal ranges of any mammal, ranging from below sea level to alpine environments above 4300 meters (Hock, 1964). Previous work has shown that mice living at high and low altitudes display genetic divergence, suggesting that natural selection is driving altitudinal divergence between populations (Storz & Dubach, 2004).

An increased hemoglobin affinity for oxygen in deer mice living at high altitudes has been demonstrated to be associated with cold and hypoxic conditions (Snyder et al., 1982; Storz, 2007; Storz et al., 2009), along with other morphological and physiological traits, including higher ventilation rates (Chappell, 1985; Hammond et al., 1999; Cheviron et al., 2013). Several of these traits, such as increased aerobic performance, hemoblobin amounts, and hematocrits, are developmentally plastic, occurring over the course of a single lifetime (Hammond et al., 2002; Cheviron et al., 2013).

Most of the high altitude adaptations that have been described for humans and other species physiological or genetic in nature, rather than morphological. Furthermore, most of the literature on high-altitude adaptations has understandably emphasized the impacts of hypoxia. Much less research has been conducted on adaptations to the combination of decreased aridity and low temperatures at high altitude. Although hypoxia has selected for increased ventilation rates, these will likely lead to higher rates of heat and water loss in an environment that is relatively cool and dry. This raises the question: are there morphological adaptations in deer mice to mitigate heat and water loss at high altitude?

In mammals, the nasal cavity houses the turbinals, a set of bones that have a dual role in olfaction and respiration. The respiratory turbinals (often comprised of the maxilloturbinals) are covered by a nonsensory mucosal layer and serve to retain heat and water during ventilation. As cold, dry air enters the nose, it draws heat and moisture from the nasal epithelium, and rapidly reaches body temperature and full saturation before entering the respiratory tract. Upon exhalation, the respiratory turbinal mucosal layer now draws heat and water from the relatively warm and wet expired air. Nasal countercurrent airflow assists in the retention of heat and water (Jackson and Schmidt-Nielsen, 1964; Schmidt-Nielsen et al, 1970), and this mechanism is found

in all mammals to various degrees (Negus, 1958), with the possible exception of cetaceans given their significantly reduced turbinals (Berta, 2014). In desert-dwelling animals, the challenge of water retention is often handled through reduced evaporative water loss, including hyperthermia (Walsberg, 2000) as well as nasal countercurrent airflow. This system has already been shown to have a significant role in heat and water retention in small rodents, including *Peromyscus leucopus*, the white-footed mouse (Getz, 1968).

Previous work has demonstrated significant functional associations between respiratory turbinal size and major ecological groupings based on the degree of heat and water stress in the organism's environment (Van Valkenburgh, 2011). However, comparative studies of turbinal morphology have tended to be performed at the interspecific or higher taxonomic levels (Van Valkenburgh, 2011; Ruf, 2014; Van Valkenburgh et al., 2014; Yee et al., 2016). This likely follows from the fact that gross turbinal complexity tends to differ between, but not within, broad taxonomic groups such as families or orders (Negus, 1958). As turbinal complexity affects relative surface area, and by extension the functional capability of the turbinals to effect heat and water exchange, this lack of variation within broad taxonomic groups is typically associated with a lack of functional variation. Comparisons of closely related sister species within the order Carnivora, which live in distinctly different environments with regards to heat and water stress, hinted at possible functional differences in respiratory turbinal size, but sample sizes were too small to test for significance (Van Valkenburgh, 2011). However, a recent study comparing two subspecies of song sparrows (Danner et al., 2017), was able to find intraspecific differences in respiratory turbinal size based on ecological groupings, suggesting that the effects of environment on respiratory morphology can be discovered at finer taxonomic scales than previously thought.

In this study, we sought to test whether turbinal morphology varies at the intraspecific level as a result of relatively extreme environment differences in mammals. Given the physiological and genetic modifications found in high-elevation dwelling rodents, we expected to see parallel modifications in skull and turbinal morphology to reflect the functional capability of the respiratory turbinals. Enhancement of nasal heat and water retention during ventilation can be achieved by increasing the surface area of the bony turbinal lattice and/or increasing air residence time in the nasal cavity. Either of these produces increased exposure to the epithelium-air interface, which allows for greater heat and water exchange. Given this, we expected to find that deer mice from high altitudes would have longer snouts and greater maxilloturbinal surface areas than deer mice from low altitudes. Turbinal surface area was quantified using high-resolution computed tomography (HRCT) scans of the snout, and geometric morphometrics were used to compare skull shape between the two populations.

METHODS

Morphometrics

P. maniculatus skulls were obtained from the Denver Museum of Nature and Science. The skulls were derived from two locations: Yuma County (1158m above sea level, n=13) and Mt. Evans (4347m above sea level, n=11) and were representatives of populations studied by J. Storz (refs). For morphometric analyses, high-resolution photographs were captured of the dorsal view of each skull using a Canon Rebel T3i camera. A ruler was included in all images for scale. A total of 14 full and semi-landmarks (Fig. 1, Table S1) were digitized using Fiji (Schindelin et al, 2012). The landmarks captured the overall shape of the skull, with particular attention paid to

the snout region. In the first round of analysis, all landmarks were included, while in the second, only the nasal landmarks were included (landmarks 1-6).

Geometric morphometrics were performed in MorphoJ (Klingenberg, 2011). Although data on the linear measurements of the skulls were available (Storz, pers. comm), a geometric morphometric analysis incorporates information on relative size, and so we did not use external linear measurements in our study. An initial analysis was performed that presumed no object symmetry and a Procrustes fit was then applied to remove the effects of size, rotation, and position. Principal components analysis (PCA) was performed on the Procrustes coordinates to visualize how shape varied across individuals as well as between the high and low altitude samples. As canonical variate analyses allows for a greater teasing apart of groups, we used canonical variate analysis (CVA) to establish if there were significant differences between the two groups. For CVA analyses, significance or lack thereof was assessed by Mahalanobis distances among groups, as opposed to Procrustes distances, because permutation tests using Mahalanobis distances do not make the same assumption of equal variance around the mean landmark that is used in standard Procrustes analysis.

The skulls were scanned at the University of Southern California Molecular Imaging Center (http://mic.usc.edu) using a nanotome computed tomography (CT) scanner. 24 specimens with fully-preserved specimens were scanned, 11 from Mt. Evans and 13 from Yuma County. For scans of turbinals, the voxel size was 27.14 μm. For scans of the entire skull, the voxel size was 9.16μm. To quantify skull measurements as well as turbinal surface area, scans of each specimen were imported into Mimics 18.0 (Materialise, Inc), a 3-D visualization software used in previous work for the purposes of turbinal surface area measurement (Green et al., 2012; Van Valkenburgh et al., 2011, 2014).

For this study, we defined the surface area of respiratory turbinals as the sum of the surface areas of the nasoturbinals and maxilloturbinals, which contributed approximately equal amounts to the total surface area. Although the nasoturbinals play a significant role in directing air to the olfactory turbinals, they are positioned just above the maxilloturbinals and appear to be well within the respiratory air flow pathway between external and internal choanae in *P. maniculatus* (Fig. 2). Turbinal surface area measurements between high-altitude and low-altitude populations were compared using a series of statistical tests in R (R Development Core Team, 2016). To correct for the effects of body mass, we used residuals from a regression of respiratory turbinal surface area (RTSA) against body size (skull length). Because the residual data set was non-normal (determined using the qqnorm function in R), we could not use conventional parametric tests such as t-tests to test for differences between the two populations. Instead, we performed a bootstrap two-group comparison in which the null hypothesis that the two groups are equal was simulated 10,000 times using the data. In each iteration of the simulation, samples are drawn from each population, and the differences between the means of the samples calculated. After 10,000 iterations, the true difference in means (from the raw data) is compared to the simulated distribution, and statistical significance is presumed if the true difference falls outside the interval that contains 95% of the simulated differences. The R code for this analysis is available on request from the author.

RESULTS

Morphometrics – Entire Skull

Based on the Procrustes ANOVA, there were no significant differences in overall skull size as estimated by centroid size between the samples from Yuma and Mt. Evans ($p=0.07$),

They also did not appear to differ significantly in shape as estimated by our landmark data. The first two principal components of an analysis of the Procrustes coordinates explained 47% of the total variance, and provided an informative analysis of shape variation with the entire sample of 24 skulls. PC3 explained another 13% of variance, but the shape change described by PC3 was uninformative, and PC3 is thus excluded from this analysis. PC1 describes a lengthening of the snout and a relative compression of the braincase (Fig. 2), while PC2 seems to describe torsion of the anterior snout. There is considerable overlap in the distribution of high and low altitude individuals on the PC plot. (Fig. 3).

Nevertheless, the CVA for the entire skull suggested that the two groups were significantly different in shape when considering Mahalanobis distances ($p<0.01$. The primary driver of the differences between groups was a lengthened snout in high-elevation deer mice. When considering Procrustes distances, however, the difference was not significant.

Morphometrics – Nasal Landmarks Only

The Procrustes ANOVA, much like the previous analysis, failed to detect a significance difference between the two groups in snout size as estimated by centroid size ($F =0.97$, $p=0.33$). However, there was a significant difference in shape ($F=2.23$, $p=0.03$). The first two principal components explained 64% of total variance, with PC3 explaining 18% of variance; once again, PC3 was discarded for being biologically non-informative. PC1 describes a relative narrowing and lengthening of the snout, with some asymmetry in the anterior portion of the snout (landmarks 2 and 3). PC2 describes a slight shortening of the snout, with the posterior section of the snout expanding slightly; however, there is notable asymmetry in the anterior portion of the

snout (Figure 4). From the PCA plot (Fig. 4), PC2 appears to somewhat separate individuals from the high and low altitude groups.

A CVA performed on the Procrustes coordinates suggested significant differences in shape between groups based on Mahalanobis distances (p=0.001). CV1 described shape change as a posterior widening and overall shortening of the snout, with asymmetry in the anterior portion yet again. Overall, regardless of whether the entire skull is considered or just the snout, low-elevation mice appear to have the aforementioned shape, while high-elevation mice seem to have overall lengthening and narrowing of the snout (with persistent asymmetry).

Respiratory Turbinal Surface Area

The bootstrap two-group comparison showed that there was a statistically significant difference between the size-corrected RTSA values between high and low-elevation groups. Higher-elevation mice had relatively higher RTSA ($p = 0.017$, Fig. 5).

DISCUSSION

In this study, we sought to identify intraspecific differences in nasal morphology in response to stressful environmental conditions. When comparing the external and internal nasal morphology of *P. maniculatus* from populations at very different altitudes, we found that there was a significantly greater relative surface area of the respiratory turbinals in the high altitude mice. This expansion of respiratory surface area is consistent with an increased demand for heat and water conservation, which is the first time such a finding has been made at the intraspecific level in mammals.

Based on the CVA, skull shape was significantly different between the high-elevation mice and low-elevation mice. Differences appear to arise primarily as a result of variability in snout length and width, with the higher-elevation mice appearing to have longer and narrower snouts. This finding is difficult to interpret, due to the conflicting implications of each result. Increased snout length would theoretically allow for increased residence time of inspired air in the nasal cavity, and consequently supports our original hypothesis. The narrower snouts, however, would potentially result in increased speed of air passing through the nasal passage, contradicting the hypothesis. The results from the morphometric analysis are thus somewhat inconclusive, and will likely require a study of flow dynamics in the nose in order to properly understand the implications of longer and narrower snouts at higher altitudes for respiration.

A quantitative comparison of the high and low altitude groups showed that deer mice from Mt. Evans had a significantly higher RTSA than those from lower elevation Yuma County, suggesting that enhanced turbinal growth occurs in response to the cold climate at higher elevation. This would represent a case of turbinal plasticity not previously described in mammals. In the case of deer mice, this finding is particularly noteworthy given that they have been known to have specific behavioral adaptations to cold temperatures, which in principle should reduce the need for compensatory turbinal growth. Such adaptations include the use of microhabitats such as burrows, where temperatures and humidity within the microclimate of a burrow are much higher than the external environment, and thus the energy budget required for homeothermy is similar in both summer and winter (Hayward, 1984). It has also been suggested that nest-building behavior of other *Peromyscus* species varies in response to the local environment, in that species inhabiting more exposed environments tend to build more robust nests that can maintain a relatively stable microclimate (Layne, 1989). Further, the ability of

Peromyscus to use microhabitats means that they are able to benefit from the insulatory properties of snow, unlike larger animals. Snow cover has previously been shown to protect smaller animals from direct exposure to adverse climatic conditions (Pruitt, 1984).

The notion that turbinal development and growth is related to environmental factors is not entirely novel. Coppola et al. (2014) previously demonstrated that intraspecific turbinal ontogenesis can be affected by environmental stimuli. In their study, turbinal development was negatively affected through unilateral nasal occlusion, suggesting a mechanical role of respiratory airflow in the proper growth of turbinals. However, the study did not address the potential role of temperature and humidity in turbinal development, which merits further investigation. Studies on the effects of environmental temperature on the appendicular skeleton have described reduced growth of the limbs of mice in cold temperatures, with some speculating that this is the result of reduced blood flow to the extremities in response to cold temperatures (Serrat et al., 2008; Serrat, 2014). As blood supply is known to be essential to proper bone growth, reduced supply to the extremities is expected to reduce bone size. The nasal turbinals, however, are highly vascularized, and have a key role in heat and water retention. Consequently, the relatively rich blood flow to the turbinals might compensate for the cold environmental air at high altitudes, resulting in relatively enhanced growth of the turbinal structure. A future experimental study that studies growth of the turbinals and perfusion of the vasculature in response to cold temperatures would be essential, and highly useful in understanding the evolution of the nasal skeleton.

TABLES AND FIGURES

Figure 2.1. All landmarks used in the morphometrics analysis.

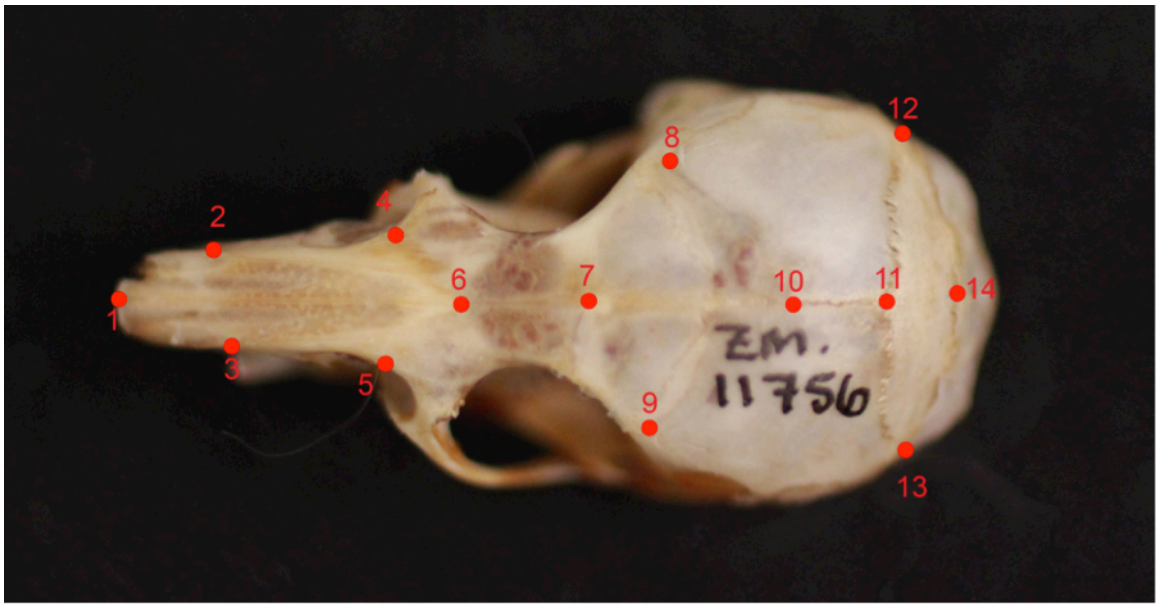

Figure 2.2. Figure 2. Positions of the nasoturbinals (blue) and maxilloturbinals (yellow) within the nasal cavity of *P. maniculatus (*DMNS 11777*),* from Yuma County.

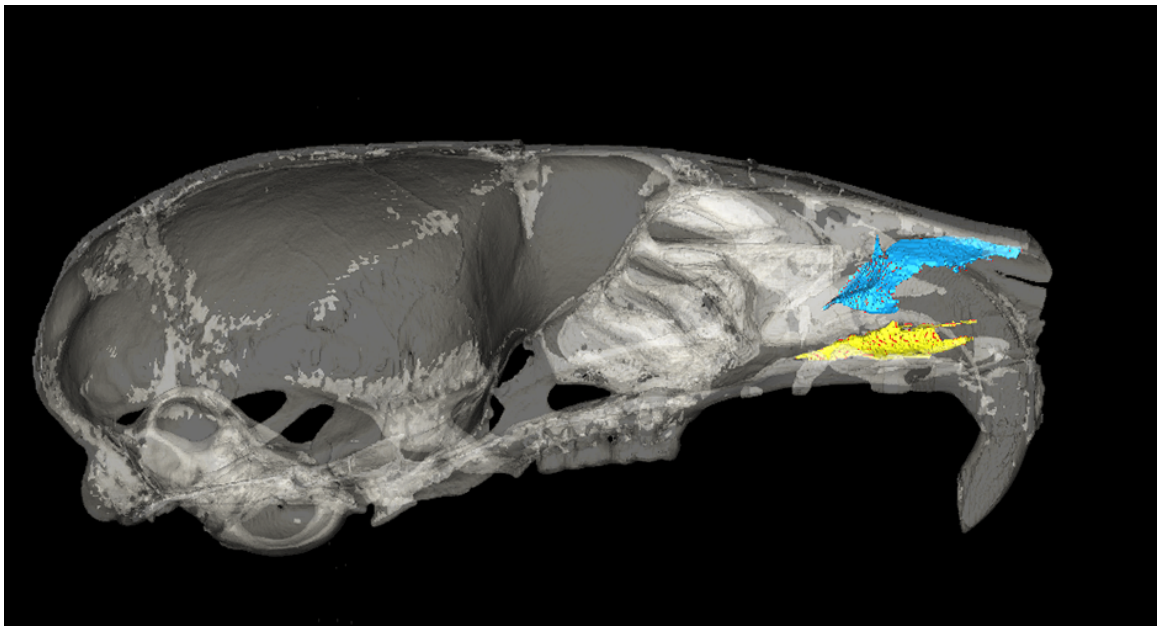

Figure 2.3. PC1 vs PC2 when considering the entire skull. High and low elevation mice are not separated clearly along either principal component.

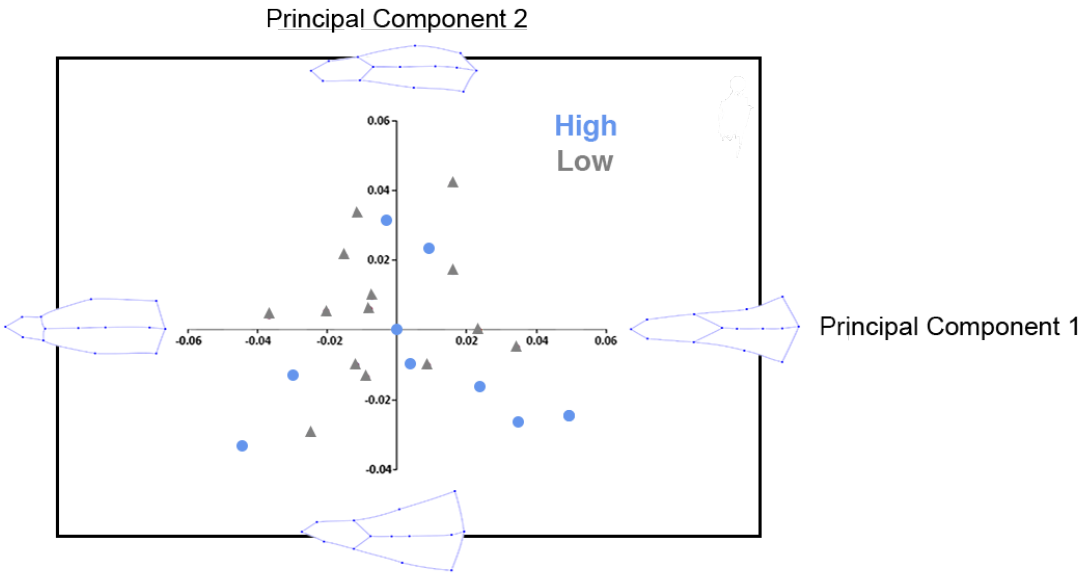

Figure 2.4. Nasal shape changes described in a plot of PC1 vs PC2. High and low elevation mice are not separated along PC1, but separated somewhat along PC2.

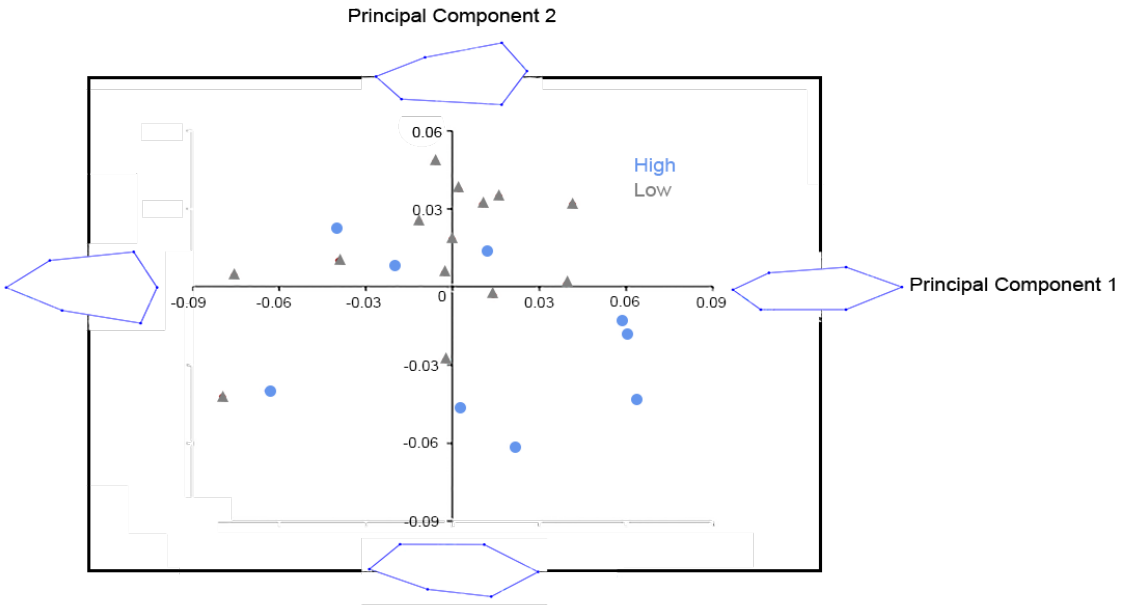

Figure 2.5. A) Linear regression of respiratory turbinal surface area against body size for all specimens. B) Boxplot of the residuals from the regression, as sorted by altitude.

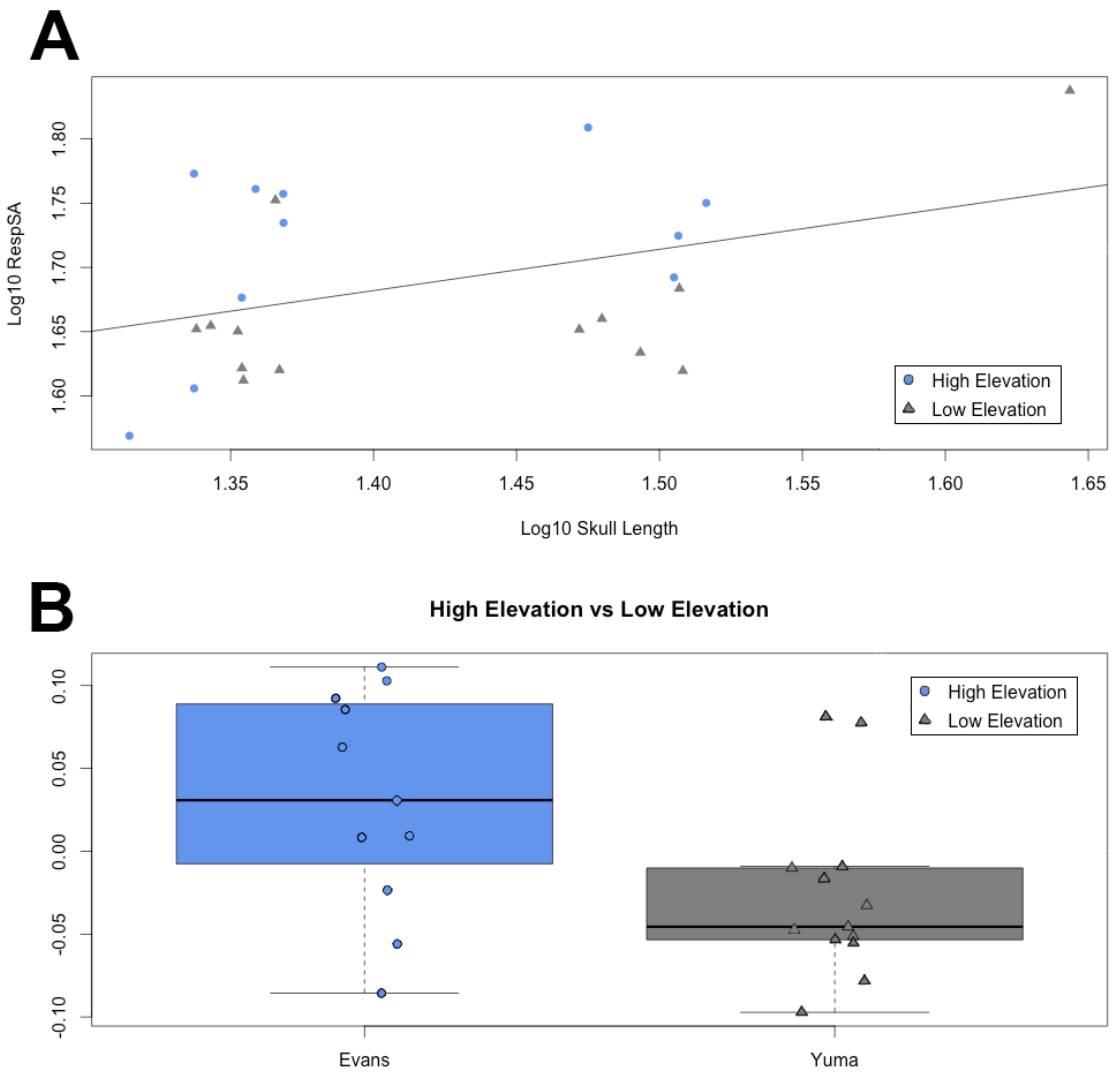

REFERENCES

Beall CM, Decker MJ, Brittenham GM, Kushner I, Gebremedhin A, Kingman PS (2002) An Ethiopian Pattern of Human Adaptation to High-Altitude Hypoxia. *Proceedings of the National Academy of Sciences of the United States of America* **99**, 17215–17218.

Beall CM (2006) Andean, Tibetan, and Ethiopian Patterns of Adaptation to High-Altitude Hypoxia. *Integrative and Comparative Biology*, **46**, 18–24.

Berta A, Ekdale EG, Cranford TW (2014) Review of the Cetacean Nose: Form, Function, and Evolution. *The Anatomical Record* **297**, 2205–2215.

Chappell MA (1985). Effects of Ambient Temperature and Altitude On Ventilation and Gas Exchange in Deer Mice (*Peromyscus maniculatus*). *Journal Of Comparative Physiology Part B: Biochemical, Systems, and Environmental Physiology*, **155**, 751–758.

Cheviron ZA, Bachman GC, Storz JF (2013). Contributions of Phenotypic Plasticity to Differences in Thermogenic Performance Between Highland and Lowland Deer Mice. *The Journal Of Experimental Biology*, **216**, 1160–1166.

Coppola DM, Craven BA, Seeger J, Weiler E (2014) The Effects of Naris Occlusion on Mouse Nasal Turbinate Development. *The Journal of Experimental Biology,* **217**, 2044-2052.

Danner RM, Gulson-Castillo ER, James HF, Dzielski SA, Frank III DC, Sibbald ET, Winker DW (2017) Habitat-Specific Divergence of Air Conditioning Structures in Bird Bills. *Auk*, **134**, 65–75.

Getz LL (1968) Relationship Between Ambient Temperature and Respiratory Water Loss of Small Mammals. *Comparative Biochemistry And Physiology*, **24**, 335–42.

Green PA, Van Valkenburgh B, Pang B, Bird D, Rowe T, Curtis A (2012) Respiratory and Olfactory Turbinal Size in Canid and Arctoid Carnivorans. *Journal of Anatomy*, **221**, 609–21.

Hammond KA, Roth J, Janes DN, Dohm MR (1999) Morphological and Physiological Responses to Altitude in Deer Mice *Peromyscus maniculatus*. *Physiological and Biochemical Zoology*, **72**, 613-622.

Hammond KA, Chappell MA, Kristan DM (2002) Developmental Plasticity in Aerobic Performance in Deer Mice (*Peromyscus maniculatus*). *Comparative Biochemistry and Physiology Part A: Molecular & Integrative Physiology*, **133**, 213-224.

Hayward JS (1965) Microclimate Temperature and its Adaptive Significance in Six Geographic Races of Peromyscus. *Canadian Journal of Zoology*, **43**, 341–50.

Hock, R (1964) Physiological Responses of Deer Mice to Various Native Altitudes. *The Physiological Effects of High Altitude* (ed. W. H. Weihe). New York, NY: Macmillan.

Jackson DC, Schmidt-Nielsen K (1964) Countercurrent Heat Exchange in the Respiratory Passages. *Proceedings of the National Academy of Sciences of the United States of America*, **51**, 1192–1197.

Janecka JE, Nielsen SSE, Andersen SD, Hoffmann FG, Weber RE, Anderson T, Storz JF, Fago A (2015) Genetically Based Low Oxygen Affinities of Felid Hemoglobins: Lack of Biochemical Adaptation to High-Altitude Hypoxia in the Snow Leopard. *The Journal of Experimental Biology*, **218**, 2402–2409.

Klingenberg CK (2011) MorphoJ: An Integrated Software Package for Geometric Morphometrics. *Molecular Ecology Resources*, **11**, 353-357.

Layne JN (1969) Nest-Building Behavior in Three Species of Deer Mice, Peromyscus. *Behavior,* **3**, 288–302.

Natarajan C, Projecto-Garcia J, Moriyama H, Weber RE, Muñoz-Fuentes V, Green AJ, Kopuchian C, Tubaro PL, Alza L, Bulgarella M, Smith MM, Wilson RE, Fago A, McCracken KG, Storz JF (2015) Convergent Evolution of Hemoglobin Function in High-Altitude Andean Waterfowl Involves Limited Parallelism at the Molecular Sequence Level. *PLoS Genetics*, **11**, 1–25.

Negus, VE (1958). *The Comparative Anatomy and Physiology of the Nose and Paranasal Sinuses*, Livingstone, London.

Pang B, Yee KK, Lischka FW, Rawson NE, Haskins ME, Wysocki CJ, Craven BA, Van Valkenburgh B (2016). The Influence of Nasal Airflow on Respiratory and Olfactory Epithelial Distribution in Felids. *The Journal of Experimental Biology*, **219**, 1866-1874.

Projecto-Garcia J, Natarajan C, Moriyama H, Weber RE, Fago A, Cheviron ZA, Dudley R, McGuire JA, Witt CC, Storz JF (2013) Repeated Elevational Transitions in Hemoglobin Function During the Evolution of Andean Hummingbirds. *Proceedings of the National Academy of Sciences of the United States of America*, **110**, 20669–20674.

Pruitt WO (1984) Snow and Small Mammals. *Winter Ecology of Small Mammals*, eds Merritt JF, International Colloquim on Winter Ecology (Carnegie Museum of Natural History, Pittsburgh), pp 1–8.

R Core Team (2016). R: A Language and Environment for Statistical Computing. R Foundation for Statistical Computing, Vienna, Austria. URL https://www.R-project.org/.

Reynafarje C, Faura J, Villavicencio D, Curaca A, Reynafarje B, Oyola L, Contreras L, Vallenas E, Faura A (1975) Oxygen Transport of Hemoglobin in High-Altitude Animals (Camelidae). *Journal of Applied Physiology,* **38**, 806–810.

Revsbech IG, Tufts DM, Projecto-Garcia J, Moriyama H, Weber RE, Storz JF, Fago A (2013) Hemoglobin Function and Allosteric Regulation in Semi-Fossorial Rodents (Family Sciuridae) With Different Altitudinal Ranges. *The Journal of Experimental Biology*, **216**, 4264–4271.

Ruf I (2014) Comparative Anatomy and Systematic Implications of the Turbinal Skeleton in Lagomorpha (Mammalia), *The Anatomical Record*, **297**, 2031–2046.

Schindelin J, Arganda-Carreras I, Frise E, Kaynig V, Longair M, Pietzsch T, Preibisch S, Rueden C, Saalfeld S, Schmid B, Tinevez JY, White DJ, Hartenstein V, Eliceiri K, Tomancak P, Cardona A (2012) Fiji: An Open-Source Platform for Biological-Image Analysis. *Nature Methods*, **9***,* 676-682.

Schmidt-Nielsen K, Hainsworth FR, Murrish DE (1970). Counter-Current Heat Exchange in the Respiratory Passages: Effect on Water and Heat Balance. *Respiration Physiology*, **9**, 263–76.

Serrat MA, King D, Lovejoy CO (2008) Temperature Regulates Limb Length in Homeotherms by Directly Modulating Cartilage Growth. *Proceedings of the National Academy of Sciences of the United States of America*, **105**, 19348–19353.

Serrat MA (2014) Environmental Temperature Impact on Bone and Cartilage Growth. *Comprehensive Physiology*, **4**, 621–655.

Snyder LRG, Born S, Lechner AJ (1982) Blood Oxygen Affinity in High- and Low-Altitude Populations of the Deer Mouse. *Respiration Physiology*, **48**, 89–105.

Storz JF, Dubach JM (2004) Natural Selection Drives Altitudinal Divergence at the Albumin Locus in Deer Mice, *Peromyscus maniculatus*. *Evolution*, **58**, 1342–1352.

Storz JF (2007) Hemoglobin Function and Physiological Adaptation to Hypoxia in High-Altitude Mammals. *Journal of Mammalogy*, **88**, 24–31.

Storz JF, Runck AM, Sabatino SJ, Kelly JK, Ferrand N, Moriyama H, Weber RE, Fago A (2009) Evolutionary and Functional Insights into the Mechanism Underlying High-Altitude Adaptation of Deer Mouse Hemoglobin. *Proceedings of the National Academy of Sciences of the United States of America*, **106**, 14450–11455.

Van Valkenburgh B, Curtis A, Samuels JX, Bird D, Fulkerson B, Meachen-Samuels J, Slater GJ (2011) Aquatic Adaptations in the Nose of Carnivorans: Evidence from the Turbinates. *Journal of Anatomy*, **218**, 298-310.

Van Valkenburgh B, Pang B, Curtis A, Yee KK, Wysocki CJ, Craven BA (2014) Respiratory and Olfactory Turbinals in Feliform and Caniform Carnivorans: The Influence of Snout length. *The Anatomical Record*, **297**, 2065-2079.

Walsberg GE (2000) Small Mammals in Hot Deserts: Some Generalizations Revisited. *BioScience*, **50**, 109-120.

Yee KK, Craven BA, Wysocki CJ, Van Valkenburgh B (2016) Comparative Morphology and Histology of the Nasal Fossa in Four Mammals: Gray Squirrel, Bobcat, Coyote, and White-Tailed Deer. *The Anatomical Record*, **299**, 840-852.

CHAPTER 3

Optimality in Respiratory Turbinal Size in Carnivorans and Ungulates: A Comparative Study

Introduction

The idea of optimal trait values suggests that for a given trait, there is a natural optimum (or range of optimum values) towards which adaptive evolution will trend in a given environment. This idea underlies concepts such as the Ornstein-Uhlenbeck model of trait evolution, which has been applied to the study of adaptive evolution (Hansen et al., 2008; Beaulieu et al., 2012). Obstacles to approaching the optimum trait value, however, include pleiotropy (Welch & Waxman, 2003; Orr, 2008; Guillame & Otto, 2012) and the need for tradeoffs between competing adaptations (MacIver et al., 2012), among other factors. Depending on the degree of the tradeoff required, or the strength of pleiotropic relationships, it is easy to understand why some traits may not necessarily converge upon a single optimum. However, there may be some traits for which these constraints are minimal, and where there is a clear signal of selection towards an optimum trait value. This might be expected in cases where the size of a feature, such as surface area of the digestive system, is strongly determined by another feature, such as overall body mass. A possible example of such a trait is the surface area of the respiratory turbinals within the mammalian skull, due to their key role in limiting heat and water loss during ventilation.

The snouts of mammals house a complex set of paper-thin bones known as the maxilloturbinals or respiratory turbinals that are covered with a well-vascularized, moist epithelium. As noted above, the expanded surface area provided by maxilloturbinals functions to reduce the loss of body heat and water that occurs as a result of lung ventilation (Negus, 1958).

Given this, the maxilloturbinals have been suggested to have had a significant role in the origin of endothermy in mammals because of the need for enhanced ventilation rates (Hillenius, 1992, 1994). According to Negus (1958), the architecture of the maxilloturbinals tends to vary among mammals belonging to different phylogenetic groups. In ungulates, the shape of the maxilloturbinals is relatively simple and described as "double-scrolled", whereas in carnivorans, maxilloturbinal shape is more complex and described as "branching" (Fig. 1). It is possible that reduced maxilloturbinal complexity is associated with a reduced ability to recover heat and water when breathing. However, Negus (1958) argued that the maxilloturbinals of ungulates achieve the same functional capacity "by length rather than by branching", suggesting a possible role of snout length in ungulates. This idea was supported by Ranslow et al. (2014), who found that the maxilloturbinal in a deer occupied a larger proportion of the length of the nasal fossa compared with carnivorans. However, neither of the above two studies compared the surface area of the maxilloturbinals relative to body size in ungulates and carnivorans and so it is not clear whether there is a convergence upon similar functional capacity in ungulates and carnivorans.

In this study, we were interested in assessing whether the scaling of maxilloturbinal surface area with body size differed significantly between ungulates and carnivores. If both groups have converged on similar proportions of respiratory turbinal surface area to body mass despite their marked differences in morphology and ecology, then this would support a tight functional relationship between maxilloturbinal size and respiratory function. Because we are interested in exploring this relationship in fossil mammals in the future, we also examined the relationship between turbinal surface area and two previously established cranial proxies for body mass, skull length and occiput to orbit length (Van Valkenburgh, 1990; Pang et al., 2016).

The latter measure excludes the rostrum and may be a better proxy in this case due to apparent differences in relative snout length between our two groups.

We also explored whether diet played a role in shaping the size of respiratory turbinals in ungulates. The functional significance of the respiratory turbinals has been well-studied in a number of living ungulates, including camels (Langman, 1978), giraffes (Langman, 1979), reindeer (Langman, 1985), antelope (Kamau et al., 1984), and a swath of domesticated species such as pigs, sheep and cows (Schroter & Watkins, 1989). In these animals, the respiratory turbinals have a significant role in heat and water retention; for example, in the reindeer, up to 75-80% of the heat and water added to each breath is retained and this has significant metabolic implications for survival (Langman. 1985). Broadly speaking, the three dietary categories into which ungulates can be sorted are as follows: grazers (>90% grassy plants), mixed feeders (10-90% grassy plants) and browsers (>90% leaves or fruits) (Hoffman & Stewart, 1972). It has been previously established that the water content of forage affects dependence on external water sources (Jarman, 1973), and that the lower water content in the diet of grazing animals makes them relatively more dependent on water sources compared to browsers (Maloiy, 1973a; Kay, 1997). Given the role of the respiratory turbinals in water conservation for ungulates, we thus expected to find that grazing ungulates should have relatively larger maxilloturbinals compared to browsers and mixed feeders, while mixed feeders should have relatively larger maxilloturbinals compared to browsers.

In order to address these two questions, we quantified respiratory turbinal surface area using high-resolution computed tomography (HRCT) scans of skulls. Ungulates and carnivorans were then compared using a series of regression and residual analyses, using measures of body

size that were both snout-dependent and snout-independent. Discriminant function analysis (DFA) was then performed to determine if there were any effects of diet on respiratory turbinal size.

MATERIALS AND METHODS

The ungulate sample consisted of 21 species from two orders (Cetartiodactyla and Perissodactyla). In total, 8 families were represented by one to six species each: Antilocapridae (1), Bovidae (6), Camelidae (2), Cervidae (3), Suidae (2), Tayassuidae (3), Equidae (2), and Tapiriidae (2) (Table 3.1).

The carnivoran sample consisted of 41 species from two superfamilies, Caniformia and Feliformia. In total, 9 families were represented by one to ten species each: Mephitidae (1), Mustelidae (4), Procyonidae (2), Ursidae (3), Canidae (10), Hyaenidae (4), Herpestidae (2), Felidae (7), Viverridae (3) (Table 3.1). Data on respiratory turbinal size from these species were originally quantified in two previous studies (Van Valkenburgh et al., 2011, 2014).

Skulls were scanned at the University of Texas High Resolution X-Ray CT facility (www.ctlab.geo.utexas.edu) and were deposited on the Digimorph website (digimorph.org). For the carnivorans, two individuals were sampled when possible, one male and one female. The quantitative measurements for the two specimens were then averaged for our analyses. For the ungulates, a single individual was scanned in most cases due to the costs of scanning such large skulls All specimens were scanned twice; the entire skull was scanned first at low resolution and the region that housed the turbinals was then scanned at higher resolution. As in previous studies (Green et al., 2012; Van Valkenburgh et al., 2011, 2014), turbinal scans were first processed with custom software which applied contrast limited adaptive histogram equalization (CLAHE) (Jain,

1989) to increase the contrast between turbinal bones and air, allowing for more accurate quantification of surface area measurements.

The post-processed turbinal scans as well as skull scans were then imported into Mimics 18.0 (Materialise, Inc), a 3-D visualization software, in order to quantify respiratory turbinal surface area and to measure skull and snout length. For ungulates, we defined respiratory surface area as the surface area of the maxilloturbinals, adhering to the definition originally formulated by Negus (1958), and which has been generally used as a proxy for respiratory turbinals in other studies. Following Van Valkenburgh et al. (2014), we adjusted our definition of the respiratory turbinals in the family Felidae to include not just the maxilloturbinals, but also part of the fronto-ethmoturbinal complex which overlaps with the maxilloturbinals. This decision was further supported by the work of Pang et al. (2016), which showed that in short-snouted animals such as cats, the anterior portion of the fronto-ethmoturbinals are co-opted for respiratory function.

For all specimens, both ungulate and carnivoran, skull length was defined as the distance between the anterior margin of the central incisors, and the posterior border of the occipital condyles. Given that ungulates tend to have relatively longer snouts than carnivorans, we used a snout-independent metric of body size rather than skull length as a proxy for body size. This metric is occiput to orbit length (OOL), measured as the distance between the anterior-most rim of the orbit and the posterior border of the occipital condyles. Snout length was consequently defined as the difference between skull length and OOL. To verify that OOL was an acceptable proxy for body size, we established that there was a significant correlation between body mass as reported in the literature (Smith et al., 2003), and the OOL measurements taken in our study ($R^2 = 0.88$, $p < 0.01$).

To understand the relationship between snout length and skull length across our sample, we used the software package R (R Development Core Team, 2017) to regress the log-transformed values of snout length against skull length for all species and compared residual values between the ungulates and carnivorans. As the distributions of residuals were non-normal (assessed using the qqnorm function in R), we compared the groups using a non-parametric Wilcoxon rank-sum test. We then assessed the relationships between respiratory turbinal surface area and total skull length and OOL, respectively, using species means values for each measurement. Regressions were performed in R, and regression slope values were determined for the two groups and analyzed using the smatr package in R (Warton et al., 2012).

All ungulate species were classified into one of three dietary categories: grazers, browsers, or mixed (Table 3.1). We adhered to the dietary classifications in a previous study by Fraser and Theodor (2011), in which the authors classified an array of ungulates by diet, including the majority of the species in this study. Exceptions include *Mazama americana*, for which we referred to Gayot (2004) for a description of its diet, the two peccaries (*Pecari tajacu*, *Tayassu pecari*), for which we referred to Olmos (1993), and the bearded pig (*Sus barbatus*), for which we referred to Caldecott et al. (1993).

To assess the relative importance of body size, snout length, or respiratory turbinal surface area on dietary category, we performed a linear DFA using the MASS package in R (Venables & Ripley, 2002) to determine the linear combination of variables that was best able to separate the groups based on prior assignment to their ecological categories. We assessed the performance of the discriminant functions using the jackknife cross-validation procedure, which is recommended when sample sizes are relatively small (Dechaume-Moncharmont et al., 2011).

We also performed a MANOVA to identify which variables significantly differed between the three dietary groups. Although DFA already allows us to identify combinations of variables that best separate the groups, the MANOVA was performed to determine which specific variables showed significant differences between the three dietary categories. In the event that successful discriminant functions were multivariate, the MANOVA provides an indication of which variables are of greatest significance. For any significant or potentially significant variables, a Wilcoxon ranked-sum test was conducted to determine which dietary groups differed from each other.

RESULTS

Snout length comparisons

Across the combined sample of carnivorans and ungulates, snout length scaled with significant positive allometry to skull length (slope = 1.44 $p < 0.01$) (Table 3.2, Fig. 2A). The same was true within carnivorans ($p<0.01$), caniforms ($p<0.01$) and feliforms ($p=0.02$). Notably, ungulate snouts did not scale with positive allometry, but rather isometry (slope = 1.11 $p>0.05$). When only artiodactyls were considered, however, the scaling relationship was significantly positively allometric (slope = 1.23 $p=0.005$). The change in slope is largely due to the removal of the tapirs, both of which had relative snout lengths that were more similar to canids than other ungulates. Based on the analysis of residual values, ungulates had significantly larger relative snout lengths than all carnivorans ($p<0.01$,Table 3.2). Within carnivorans, caniforms had larger relative snout lengths than feliforms ($p<0.01$), but were still significantly shorter than those of ungulates ($p<0.05$).

Respiratory Turbinal Surface Area in Relation to Body Mass

Across all species, RSA scaled with isometry (slope = 0.69, p =0.72)(Table 3.2, Fig. 3) Ungulates also scaled with isometry (slope = 0.63, p=0.86), although artiodactyls alone scaled with significant positive allometry (slope=0.72, p=0.02 (Table 3.2). Carnivorans also scaled with significant positive allometry (slope=0.83, p<0.001), and did not differ significantly from the scaling relationship observed in artiodactyls (p=0.40). Residual comparisons showed that mean relative RSA was slightly larger in carnivorans than ungulates v but the difference was not significant (p=0.055, Figure 4). The variance in relative RSA values was much greater in ungulates than carnivorans. Notable outliers with relatively reduced RSA included *Tapirus bairdii* (TBA), as well as *Lama guanicoe* (LGU), *Pecari tajacu* (PTA) and *Madoqua guentheri* (MGU) (Fig. 3). The one outlier that had high relative RSA for its size was the reindeer, *Rangifer tarandus* (RTA).

Respiratory Turbinal Surface Area in Relation to OOL

Across the combined sample of carnivorans and ungulates, RSA scaled with significant positive allometry (slope = 2.74 p<0.01) (Table 3.2, Fig. 2B). This was largely driven by the strong positive allometry of carnivoran RSA (p=<0.01). Surprisingly, ungulates scaled isometrically (p=0.72), but if perissodactyls were removed, the scaling relationship based on artiodactyls alone was positively allometric (p=0.01), but did not significantly differ from carnivorans. Again, the tapirs (TBA,TTE in Fig. 2B) were outliers with relatively reduced RSA. Based on the residuals of the RSA-OOL regression for the entire sample, ungulates had a marginally greater but non-significant (p=0.79) relative RSA than carnivorans.

Respiratory Turbinal Surface Area in Relation to Skull Length

RSA scaled isometrically with skull length ($p=0.86$) across all 62 species (slope =2.03) as well as within ungulates (slope= 2.12, $p=0.78$). (Table 3.2). In both carnivorans and artiodactlys, RSA scaled with significant positive allometry ($p<0.05$). Analysis of the residual values for the regression across all species revealed that that carnivorans had higher RSA for their skull length than ungulates ($p<0.05$), even when perissodactyls were excluded ($p<0.05$). The difference appeared to be driven largely by the short-snouted feliforms; when comparing all ungulates to caniforms, the difference fell just short of statistical significance ($p=0.054$).

Discriminant Function Analysis for Dietary Comparisons among Ungulates

The DFA showed that the most successful model was one that only required relative RSA, with a 60% success rate. The two next most successful models both had a 55% success rate; one model included all three variables, while the other included both RSA and OOL (Table 3.3). The MANOVA found that none of the three variables differed significantly between all three groups (Table 4), although relative RSA came close ($p=0.09$). When comparing mean relative RSA between the dietary groups, browsers had the least RSA, followed by grazers, and then mixed feeders, but the differences between the groups were not significant (Fig. 4b). However, the difference between browsers and -mixed feeders approached significance ($p=0.055$). When only artiodactyls were considered, this trend vanished, suggesting that the browsing perissodactyls may have played a role in driving the previous trend.

DISCUSSION

In this study, we sought to answer two questions, the first of which was whether respiratory turbinal size would converge upon an optimal range, across distantly related species. We first determined that ungulate snouts, as a proportion of the entire skull, were in fact longer than those of carnivorans (Table 3.2). Snout lengths were also shown to play a significant role in measuring relative RSA size. When skull length was used as a proxy for body size, carnivorans had a significantly greater RSA than ungulates. This was likely due in large part to the felids, in which relative RSA is artificially high owing to the shortened snout. In contrast, when body mass or OOL, both snout-independent metrics were used as a proxy for body size, there was no significant difference between the relative RSA of ungulates compared to carnivorans. Further, the scaling relationship of RSA to body mass did not differ significantly between ungulates and carnivorans, suggesting that there is a very similar relationship between RSA and body mass in these two groups. This supports our hypothesis that there may be an evolution to an optimum relative RSA in both carnivorans and ungulates. Convergence upon mechanically optimal solutions given similar morphology has previously been demonstrated in a locomotor context (Bale et al., 2014), but our study specifically demonstrates that despite differing underlying morphology (here, respiratory turbinal shape), that distantly related species may yet converge upon similar functional capacity.

Within the ungulates, the perissodactyls, represented by two equid and two tapir species, had significantly smaller respiratory turbinals than in artiodactyls. Morphologically, the maxilloturbinals of the tapirs appeared to be simple and sheetlike, lacking the generalized double-scrolled shape described by Negus (1958) for ungulates. The reason for the reduction of turbinal complexity from an already simple shape is unclear, but care manuals for tapirs in the American Association of Zoos and Aquariums emphasize that tapirs (presumably lowland tapirs)

frequently need to cool themselves in warm weather (AZA Tapir TAG, 2013). This could be due to their extremely large body size (ranging from 150-300kg) making it relatively difficult to lose heat through thermal radiation in hot, humid environments. Thus, it is possible that selection has favored the evolution of heat-loss mechanisms in tapirs, including reductions in respiratory turbinal area.

The positive allometric scaling of ungulate snout length with respect to skull length suggests that larger ungulates have longer snouts, with a similar situation occurring in felids. Recent research has shown that within lineages, larger mammals tend to have longer faces (Cardini & Polly, 2013), and that finding is replicated here within both carnivorans and ungulates. An interesting observation to be made is that in the relatively long-snouted lion, the maxilloturbinals were double-scrolled, resembling the stereotypical ungulate condition rather than the branching patterns of most carnivorans. This is an isolated case, however, as none of the other felids had double-scrolled maxilloturbinals.

Our comparison of relative RSA among ungulates in the three different dietary groups provided mixed results. As expected, browsers tended to have lower relative RSA than either grazers or mixed feeders. Contrary to our expectations, however, mixed feeders had the highest relative RSA as opposed to grazers (Figure 4). Although there were no significant differences between dietary groups, browsers were close to differing significantly from mixed-feeders ($p=0.055$). An examination of the data, particularly the regression plot in Figure 3, suggests that this slight difference is driven by some notable outliers. Among the mixed-diet species, the reindeer (*R. tarandus*) has much higher relative RSA compared with the other ungulates in this study. As the geographic range of *R. tarandus* tends to encompass areas with notably low

temperatures such as arctic tundra, it is likely that they have enhanced RSA to further aid in heat retention, as is the case in marine as opposed to terrestrial carnivorans (ref). The guanaco (*Lama guanicoe*) represents an interesting case of a mixed feeder with an atypically small relative RSA despite living in relatively cool, dry environments. This may be due in part to the documented ability of the guanaco to significantly reduce heat loss through special behaviors such as postural changes and bedding orientations (de Lamo et al., 1988). Given these alternative ways to help retain heat, the guanaco may have reduced its reliance on the respiratory turbinals.

Among the browsers, Guenther's dik-dik (*M. guentheri*), the tapirs, and the collared peccary (*Pecari tajacu)* have smaller relative RSA compared with other ungulates in our sample. The collared peccary has previously been described as spending a substantial amount of time resting in cool places (Gongora et al., 2011); much like the tapirs, it is possible that they have evolved to prioritize heat loss as opposed to heat retention, which would explain the relatively lower RSA. The small RSA in dik-diks is unusual in that their arid habitat would typically be associated with increased water conservation demands, and consequently an increased RSA. However, there are some notable adaptations in *M. guentheri* which may reduce the importance of RSA in conserving water. Among them is their ability to have an extremely high urine concentration, and their ability to limit water loss through a reduction of cutaneous sweating (Maloiy, 1973b). Other adaptations include the storing of body heat, and reabsorption of water from feces (ibid.?). The reduced RSA in this species could thus be a function of having multiple avenues to retain water, in an analogous fashion to the reduction of RSA in the guanaco.

The majority of our discriminant functions had a low success rate at assigning specimens to the correct ecological category, with the best-performing model having a 60% success rate (Table 3.3). Although between-group comparisons of relative RSA failed to separate browsers

from grazers, is interesting to note that the better discriminant functions all incorporated relative RSA in some fashion, with the most successful model only requiring relative RSA as a single metric to separate groups. This suggests that respiratory turbinal size may yet have a closer relationship to dietary type than would otherwise be suggested by the raw data, and certainly merits further study.

TABLES AND FIGURES

Table 3.1. Species analyzed in this study and their respective dietary category. SL: Skull Length, OOL: Occiput-Orbit Length, SNL: Snout Length, RSA: Total Respiratory Surface Area

Order	Superfamily	Family	Abbr	Genus	Species	Dietary Category	SL (mm)	OOL (mm)	SNL (mm)	RSA (mm^2)
Carnivora	Caniformia	Arctoidea	MME	Mephitis	mephitis	NA	75.065	53.26905	21.79595	4622.995
Carnivora	Caniformia	Arctoidea	GGU	Gulo	gulo	NA	162.93	102.1908	60.7392	13910.46
Carnivora	Caniformia	Arctoidea	MFR	Mustela	frenata	NA	45.025	35.35715	9.66785	679.505
Carnivora	Caniformia	Arctoidea	NVI	Neovison	vison	NA	73.51	59.96	13.55	2343.06
Carnivora	Caniformia	Arctoidea	TTA	Taxidea	taxus	NA	125.39	82.15	43.24	8645.315
Carnivora	Caniformia	Arctoidea	PFL	Potos	flavus	NA	88.08	65.65825	22.42175	3721.76
Carnivora	Caniformia	Arctoidea	PLO	Procyon	lotor	NA	121.785	76.7354	45.0496	10848.89
Carnivora	Caniformia	Arctoidea	UAM	Ursus	americanus	NA	246.58	154.2651	92.3149	57494.7
Carnivora	Caniformia	Arctoidea	UAR	Ursus	arctos	NA	348.47	221.3915	127.078	143009.2
Carnivora	Caniformia	Arctoidea	UMA	Ursus	maritimus	NA	384.815	273.2206	111.5944	175243.44
Carnivora	Caniformia	Canidae	CLA	Canis	latrans	NA	177.98	102.505	75.475	16021.89
Carnivora	Caniformia	Canidae	CLUb	Canis	lupus baileyi	NA	236.11	121.6016	114.5084	20491.01
Carnivora	Caniformia	Canidae	LPI	Lycaon	pictus	NA	194.41	112.8986	81.5114	19089.34
Carnivora	Caniformia	Canidae	NPR	Nyctereutes	procyonoides	NA	119.2575	71.30565	47.9518	7641.59
Carnivora	Caniformia	Canidae	OME	Otocyon	megalotis	NA	124.28	71.84845	52.4315	5564.68
Carnivora	Caniformia	Canidae	SVE	Speothos	venaticus	NA	130.02	94.5	35.52	5639.8
Carnivora	Caniformia	Canidae	UCI	Urocyon	cinereoargenteus	NA	112.38	73.59	38.79	3790.78
Carnivora	Caniformia	Canidae	VLA	Vulpes	lagopus	NA	129.44	84.745	44.695	8486.99
Carnivora	Caniformia	Canidae	VMA	Vulpes	macrotis	NA	106.0045	70.215	35.7895	4233.05
Carnivora	Caniformia	Canidae	VVU	Vulpes	vulpes	NA	137.96	82.45	55.51	7046.23
Carnivora	Feliformia	Hyaenidae	CCR	Crocuta	crocuta	NA	232.4765	153.533	78.9425	71903.32
Carnivora	Feliformia	Hyaenidae	PBR	Parahyaena	brunnea	NA	232.9345	148.7642	84.1707	65645.97
Carnivora	Feliformia	Hyaenidae	HHY	Hyaena	hyaena	NA	209.3804	132.9175	76.4629	59505.1
Carnivora	Feliformia	Hyaenidae	PCR	Proteles	cristata	NA	137.288	88.0877	49.2003	14473.96
Carnivora	Feliformia	Herpestidae	GSA	Galerella	sanguinea	NA	61.0542	47.3332	13.721	857.62
Carnivora	Feliformia	Herpestidae	SSU	Suricatta	suricatta	NA	57.92125	41.03455	16.8867	854.02
Carnivora	Feliformia	Felidae	PPA	Panthera	pardus	NA	215.55	159.66	55.89	62801.12
Carnivora	Feliformia	Felidae	LPA	Leopardus	pardalis	NA	125.3699	98.7572	26.6127	19077.2
Carnivora	Feliformia	Felidae	LRU	Lynx	rufus	NA	109.4429	86.909	22.53395	14263.99

Carnivora	Feliformia	Felidae	AJU	Acinonyx	jubatus	NA	166.2749	116.2657	50.0092	56745.89
Carnivora	Feliformia	Felidae	PCO	Puma	concolor	NA	178.8177	125.9195	52.8983	40049.11
Carnivora	Feliformia	Felidae	FSY	Felis	sylvestris	NA	79.3397	64.85955	14.48015	7961.1
Carnivora	Feliformia	Felidae	PLE	Panthera	leo	NA	278.8004	191.8803	86.92015	109995.61
Carnivora	Feliformia	Viverridae	ABI	Arctictis	binturong	NA	153.0211	106.6656	46.3555	11742.9
Carnivora	Feliformia	Viverridae	NBI	Nandinia	binotata	NA	87.8343	63.7131	24.1212	3363.7
Carnivora	Feliformia	Viverridae	PLI	Prionodon	linsang	NA	73.8808	53.1894	20.6914	1213.16
Ungulata	Artiodactyla	Antilocapridae	AAM	Antilocapra	americana	Mixed	278.5266	98.8548	179.6718	61193.8
Ungulata	Artiodactyla	Bovidae	MGU	Madoqua	guentheri	Browser	89.7508	49.7138	40.037	1295.6
Ungulata	Artiodactyla	Bovidae	RAR	Redunca	arundinum	Grazer	271.0008	124.8477	146.1531	36272.42
Ungulata	Artiodactyla	Bovidae	RRU	Rupicapra	rupicapra	Mixed	203.6873	95.1379	108.5494	29468.62
Ungulata	Artiodactyla	Bovidae	STA	Saiga	tatarica	Mixed	221.9157	101.1222	120.7935	22023.9
Ungulata	Artiodactyla	Bovidae	TSC	Tragelaphus	scriptus	Browser	208.7451	112.6176	96.1275	20443.68
Ungulata	Artiodactyla	Bovidae	DLU	Damaliscus	lunatus	Grazer	383.1498	143.4763	239.6735	70040.34
Ungulata	Artiodactyla	Camelidae	LGU	Lama	guanicoe	Mixed	287.9323	137.0247	150.9076	25329.44
Ungulata	Artiodactyla	Camelidae	VVI	Vicugna	vicugna	Mixed	272.2144	132.2221	139.9923	25162.06
Ungulata	Artiodactyla	Cervidae	MAM	Mazama	americana	Browser	207.2426	106.4312	100.8114	19334.82
Ungulata	Artiodactyla	Cervidae	OHE	Odocoileus	hemionus	Browser	288.2055	135.4418	152.7632	75699.7
Ungulata	Artiodactyla	Cervidae	RTA	Rangifer	tarandus	Mixed	388.1405	158.3136	229.8269	175615.66
Ungulata	Artiodactyla	Suidae	SBA	Sus	barbatus	Mixed	389.1361	110.6095	278.5266	62308.18
Ungulata	Artiodactyla	Suidae	PAE	Phacochoerus	aethiopicus	Grazer	52.7501	20.5736	32.1765	70122.76824
Ungulata	Artiodactyla	Tayassuidae	PTA	Pecari	tajacu bangsi	Browser	203.9162	81.3032	122.6130	6040.32
Ungulata	Artiodactyla	Tayassuidae	PTA	Pecari	tajacu crusnigrum	Browser	197.7777	81.8788	115.8989	4240.98
Ungulata	Artiodactyla	Tayassuidae	TPE	Tayassu	pecari spiradens	Browser	231.6972	91.8868	139.8104	25369.18
Ungulata	Perissodactyla	Equidae	EBU	Equus	burchelli beoni	Grazer	465.7765	197.7025	268.0735	57050.62
Ungulata	Perissodactyla	Equidae	EGR	Equus	grevyi	Grazer	584.9107	222.8262	362.0845	72617.18
Ungulata	Perissodactyla	Tapiridae	TBA	Tapirus	bairdii	Browser	381.5802	217.7186	163.8616	7747.108594
Ungulata	Perissodactyla	Tapiridae	TTE	Tapirus	terrestris	Browser	388.9442	226.9245	162.0197	35910.73654

Table 3.2. Regression slope values and residual comparisons between groups.

Regression	All species	Ungulates only	Artiodactyls only	Carnivorans only
SNL vs SL	1.44*	1.11	1.23*	1.3*
RSA vs OOL	2.74*	1.8	3.69*	3.16*
RSA vs SL	2.03	2.12	3.04*	2.74*
RSA vs Mass	0.69	0.63	0.72*	0.83*

* refers to significant positive allometry

Residual Comparisons	Ungulata vs Carnivora	Ungulata vs Felifomia	Ungulata vs Caniformia	Caniformia vs Feliformia
SNL vs SL	**0.0001**	NA	**0.02**	**0.002**
RSA vs OOL	0.79	0.59	0.91	0.1
RSA vs SL	**0.002**	**0.0008**	0.054	**0.017**
RSA vs Mass	0.055	**0.03**	0.25	0.09

Bolded values refer to significant differences between groups

Table 3. Discriminant Function Analysis models and the success rate of assigning species to ecological categories. RelSNL: Relative Snout Length, OOL: Occiput-Orbit Length, RSA: Relative Respiratory Surface Area

Group	Model	Correct classification rate (%)
Ungulate only	RelSNL + OOL + RSA	55.0%
	RelSNL + OOL	40.0%
	OOL + RSA	55.0%
	RelSNL + RSA	50.0%
	RSA	60.0%
	OOL	40.0%
	RelSNL	15.0%

Figure 3.1 Maxilloturbinal shape in a carnivoran, A) *Canis lupus* and an ungulate, B) *Rangifer tarandus*. The shape of the carnivoran maxilloturbinals are branched and complex, while the shape in an ungulate is that of a double scroll.

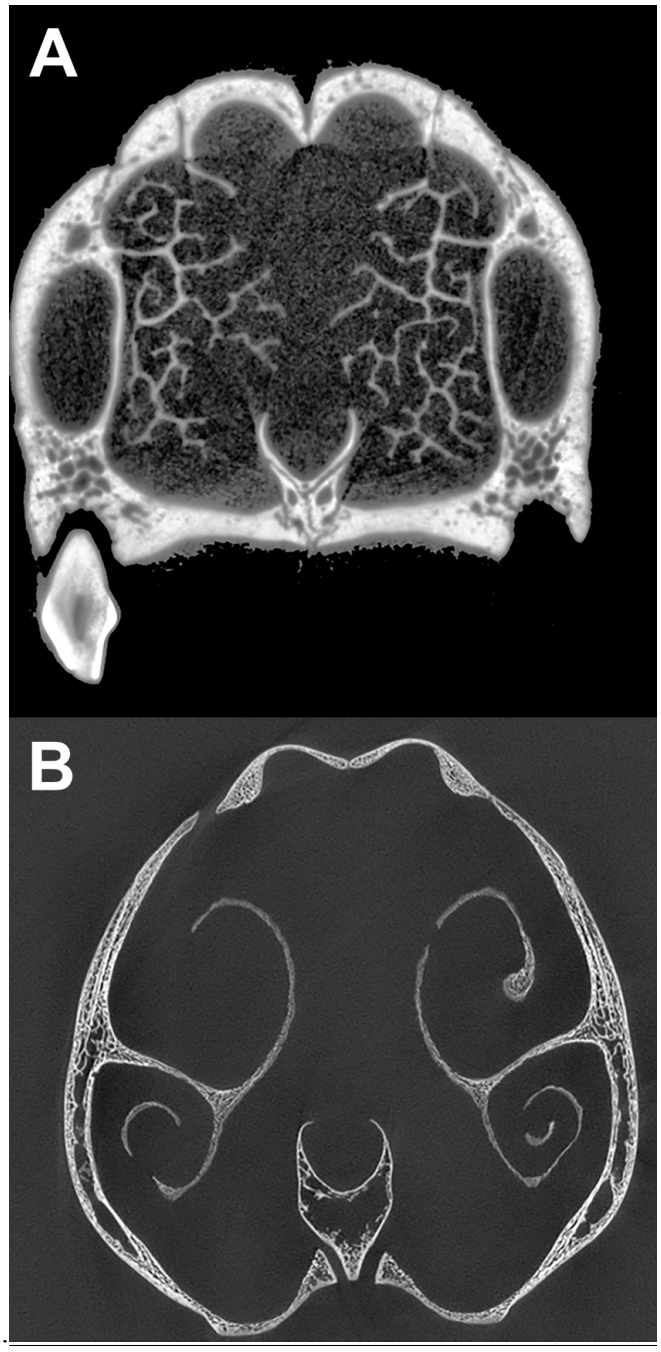

Figure 3.2 Log_{10}/Log_{10} plots of (A) Snout length against skull length, (B) Respiratory turbinal surface area (RSA) against occiput-orbit length (OOL) and (C) Respiratory turbinal surface area (RSA) against skull length. Caniforms, red diamonds; feliforms, red circles; artiodactyls, blue circles; perissodactyls, blue triangles. Regression lines for carnivorans and ungulates are in red and blue, respectively, with the regression line for artiodactyls pictured as a dashed blue line. Regression statistics are in Table 2 and species abbreviations are in Table 1.

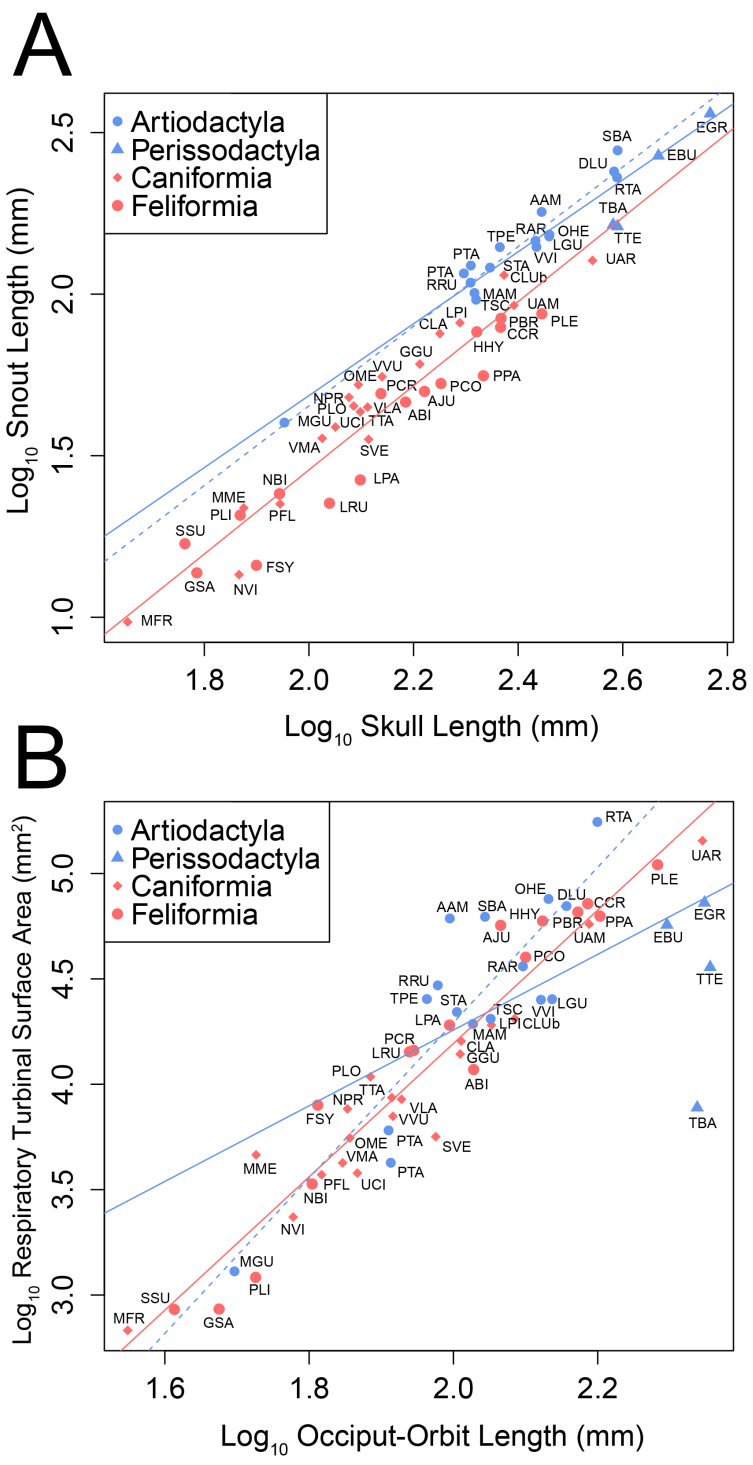
A
Artiodactyla
Perissodactyla
Caniformia
Feliformia
Log10 Snout Length (mm)
Log10 Skull Length (mm)
1.0
1.5
2.0
2.5
1.8
2.0
2.2
2.4
2.6
2.8
SBA
EGR
DLU
EBU
RTA
AAM
TBA
TPE
RAR
OHE
TTE
LGU
PTA
VVI
UAR
STA
PTA
CLUb
RRU
MAM
TSC
UAM
LPI
PBR
PLE
CLA
CCR
HHY
GGU
VVU
OME
PPA
PCR
PCO
NPR
AJU
PLO
VLA
ABI
MGU
UCI
TTA
VMA
SVE
LPA
NBI
MME
LRU
PLI
PFL
SSU
FSY
GSA
NVI
MFR
B
Artiodactyla
Perissodactyla
Caniformia
Feliformia
Log10 Respiratory Turbinal Surface Area (mm2)
Log10 Occiput-Orbit Length (mm)
3.0
3.5
4.0
4.5
5.0
1.6
1.8
2.0
2.2
RTA
UAR
PLE
OHE
DLU
CCR
AAM
SBA
HHY
PPA
EGR
PBR
AJU
UAM
EBU
RAR
PCO
TTE
RRU
TPE
STA
LGU
LPA
TSC
VVI
LPI
CLUb
MAM
PCR
CLA
LRU
GGU
PLO
ABI
TTA
NPR
TBA
VLA
FSY
VVU
SVE
OME
PTA
VMA
MME
PTA
PFL
UCI
NBI
NVI
MGU
PLI
SSU
MFR
GSA

Figure 3.3 Log_{10}/Log_{10} plot of respiratory turbinal surface area (RSA) against body mass. Caniforms, red diamonds; feliforms, red circles; artiodactyls, blue circles; perissodactyls, blue triangles. Regression lines for carnivorans and ungulates are in red and blue, respectively, with the regression line for artiodactyls pictured as a dashed blue line. Regression statistics are in Table 2 and species abbreviations are in Table 1.

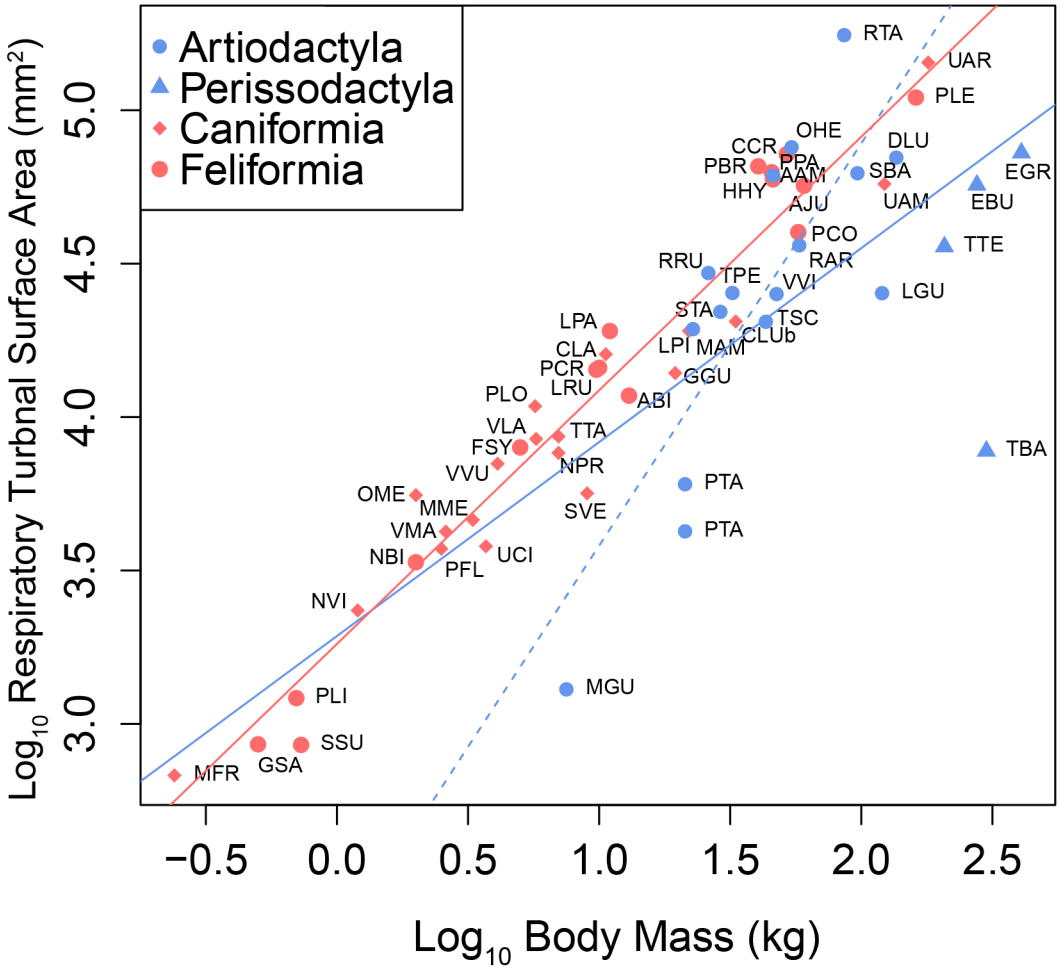

Figure 3.4 Boxplots of the residuals of the regressions of $\log_{10}$ RSA on $\log_{10}$ body mass for A) carnivorans and ungulates, and B) ungulates within the three dietary categories.

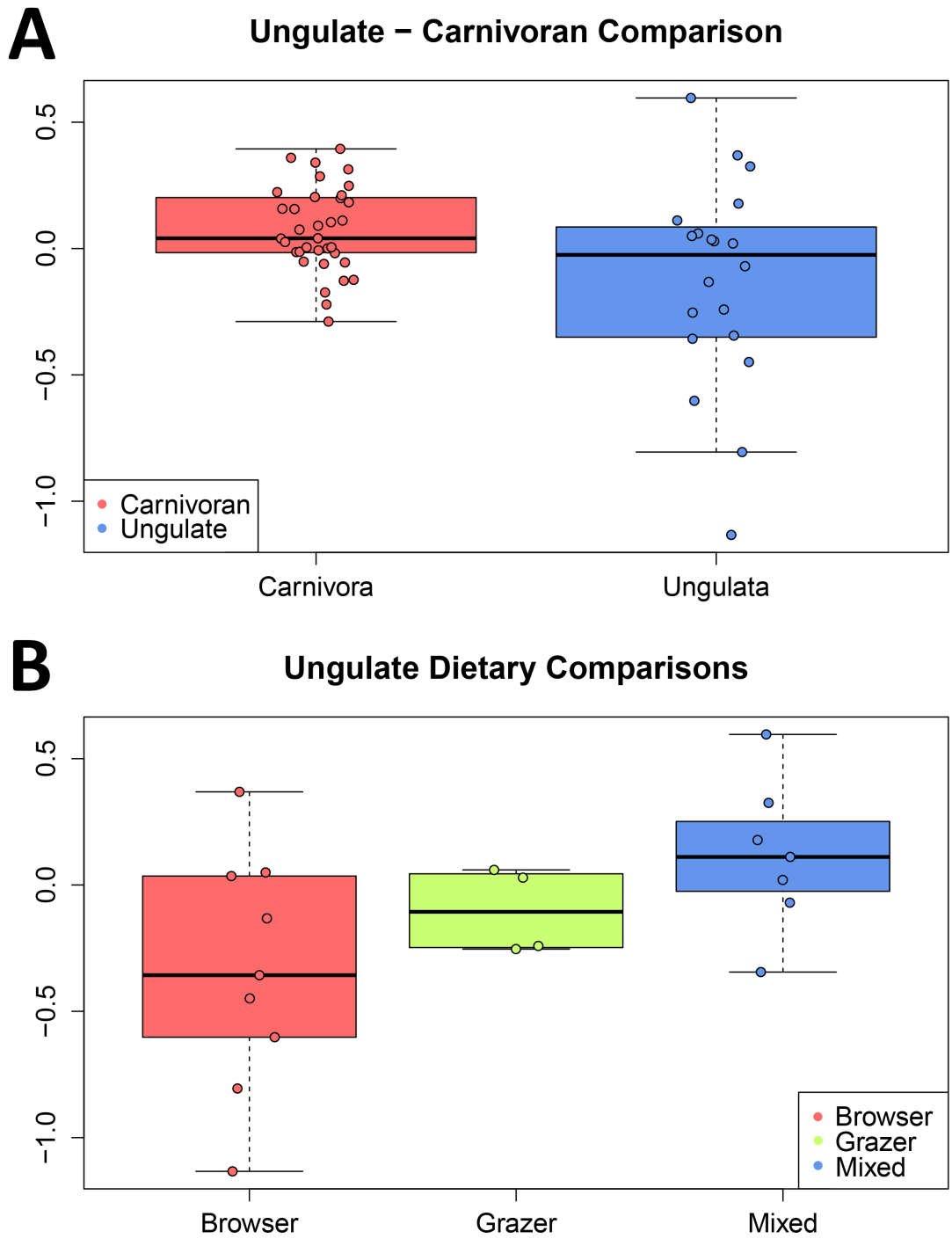

REFERENCES

AZA Tapir TAG (2013) Tapir (Tapiridae) Care Manual. *Association of Zoos and Aquariums*, **65**.

Bale R, Neveln ID, Bhalla APS, MacIver MA, Patankar NA (2015) Convergent Evolution of Mechanically Optimal Locomotion in Aquatic Invertebrates and Vertebrates. *PLoS Biology*, **13**, 1–22.

Beaulieu JM, Jhwueng DC, Boettiger C, O'Meara BC (2012) Modeling stabilizing selection: Expanding the Ornstein-Uhlenbeck model of adaptive evolution. *Evolution (N Y)*, **66**, 2369–2383.

Caldecott JO, Blouch RA, Macdonald, AA (1993) The bearded pig (*Sus barbatus*). In: Oliver, W.L.R. (Ed.) *Pigs, Peccaries and Hippos: Status Survey and Action Plan*. IUCN, Gland, Switzerland.

Cardini A, Polly PD (2013) Larger mammals have longer faces because of size-related constraints on skull form. *Nature Communications*, **4**, 1-7.

Dechaume-Moncharmont FX, Monceau K, Cezilly F (2011) Sexing Birds using Discriminant Function Analysis: A Critical Appraisal. *The Auk*, **128**, 78-86.

Fraser D, Theodor JM (2001) Comparing ungulate dietary proxies using discriminant function analysis. *Journal of Morphology* **272**, 1513-1526.

Gayot M (2004) Comparative diet of the two forest cervids of the genus Mazama in French Guiana. *Journal of Tropical Ecology*, **20**, 31-43.

Green PA, et al. (2012) Respiratory and olfactory turbinal size in canid and arctoid carnivorans. *Journal of Anatomy*, **221**, 609–621.

Guillaume F, Otto SP (2012) Gene functional trade-offs and the evolution of pleiotropy. *Genetics*, **192**, 1389–1409.

Hansen TF, Pienaar J, Orzack SH (2008) A comparative method for studying adaptation to a randomly evolving environment. *Evolution (NY)*, **62**,1965–1977.

Hillenius WJ (1992) The evolution of nasal turbinates and mammalian endothermy. *Paleobiology*, **18**,17–29.

Hillenius WJ (1994) Turbinates in therapsids: Evidence for late Permian origins of mammalian endothermy. *Evolution (NY)*, **48**, 207–229.

Hofmann RR, Stewart DRM (1972) Grazer or browser: a classification based on the stomach-structure and feeding habit of East African ruminants. *Mammalia* **36**.

Jain A (1989) *Fundamentals of Digital Image Processing.* (Prentice-Hall, Inc, Upper Saddle River, NJ). 4th Ed.

Jarman PJ (1973) The free water intake of impala in relation to the water content of their food. *East African Agricultural and Forestry Journal*, **38**, 345 – 351.

Kay RNB (1997) Responses of African livestock and wild herbivores to drought. *Journal of Arid Environments*, **38**, 683 – 694.

Langman VA, Maloiy GMO, Schmidtnielsen K, Schroter RC (1978) Respiratory Water and Heat Loss in Camels Subjected To Dehydration. *Journal of Physiol*ogy, **278**, P35–P35.

Langman VA, Maloiy G (1979) Nasal heat exchange in the giraffe and other large mammals. *Respiration Physiology*, **37**, 325–333.

Langman VA (1985) Nasal heat exchange in a northern ungulate, the reindeer (*Rangifer tarandus*). *Respiration Physiology*, **59**, 279–87.

MacIver MA, Patankar NA, Shirgaonkar AA (2010) Energy-information trade-offs between movement and sensing. *PLoS Computational Biology*, **6**, 1–12.

Maloiy GMO (1973a) Water metabolism of East African ruminants in arid and semi-arid regions. *Journal of Animal Breeding and Genetics*, **90**, 219-228.

Maloiy GMO (1973b) The water metabolism of a small East African antelope: the dik-dik. *Proceedings of the Royal Society of London*, **184**, 167-178.

Negus VE (1958) *The Comparative Anatomy and Physiology of the Nose and Paranasal Sinuses* ed Livingstone (London).

Olmos F (1993) Diet of sympatric Brazilian caatinga peccaries (Tayassu tajacu and T. pecari). *Journal of Tropical Ecology*, **9,** 255-258

Orr HA (2000) Adaptation and the Cost of Complexity. *Evolution (N Y)*, **54**, 13–20.

Pang B, Yee KK, Lischka FW, Rawson NE, Haskins ME, Wysocki CJ, Craven BA, Van Valkenburgh B (2016) The influence of nasal airflow on respiratory and olfactory epithelial distribution in felids. *Journal of Experimental Biology*, **219**,1866–1874.

R Core Team (2017). R: A language and environment for statistical computing. R Foundation for Statistical Computing, Vienna, Austria. URL https://www.R-project.org/.

Ranslow AN, Richter JP, Neuberger T, Van Valkenburgh B, Rumple CR, Quigley AP, Pang B, Krane MH, Craven BA (2014) Reconstruction and morphometric analysis of the nasal airway of the white-tailed deer (*Odocoileus virginianus*) and implications regarding respiratory and olfactory airflow. The *Anatomical Record (Hoboken)*, **297**, 2138–2147.

Schroter RC, Watkins N V (1989) Respiratory heat exchange in mammals. *Respiration Physiology*, **78**, 357–67.

Smith FA, Lyons SK, Morgan Ernest SK, Jones KE, Kaufman DM, Dayan T, Marquet PA, Brown JH, Haskell JP (2003) Body Mass of Late Quartenary Mammals. *Ecology*, **84**, 3403.

Van Valkenburgh B (1990) Skeletal and Dental Predictors of Body Mass in Carnivores. *Body Size in Mammalian Paleobiology: Estimation and Biological Implications*, eds Damuth J, MacFadden B (Cambridge University Press).

Van Valkenburgh B, Theodor J, Friscia A, Pollack A, Rowe T (2004) Respiratory turbinates of canids and felids: a quantitative comparison. *Journal of Zoology*, **264**, 281–293.

Van Valkenburgh B, Curtis A, Samuels JX, Bird D, Fulkerson B, Meachen-Samuels J, Slater GJ (2011) Aquatic adaptations in the nose of carnivorans: evidence from the turbinates. *Journal of Anatomy*, **218**, 298–310.

Van Valkenburgh B, Pang B, Bird D, Curtis A, Yee K, Wysocki C, Craven BA (2014) Respiratory and olfactory turbinals in feliform and caniform carnivorans: The influence of snout length. *The Anatomical Record*, **297**, 2065–2079.

Venables WN, Ripley BD (2002) *Modern Applied Statistics with S.* (Springer, New York). 4th Ed.

Warton DI, Duursma RA, Falster DS, Taskinen S (2012) smatr 3 - an R package for estimation and inference about allometric lines. *Methods in Ecology and Evolution*, **3**, 257–259.

Welch JJ, Waxman D (2003) Modularity and the Cost of Complexity. *Evolution (NY)*, **57**, 1723.

Yee KK, Craven BA, Wysocki CJ, Van Valkenburgh B (2016) Comparative Morphology and Histology of the Nasal Fossa in Four Mammals: Gray Squirrel, Bobcat, Coyote, and White-Tailed Deer. *The Anatomical Record*, **299**, 840–852.